1 **Landsat and Sentinel-derived glacial lake dataset in the China-**

2 **Pakistan Economic Corridor from 1990 to 2020**

4 Muchu Lesi[1], Yong Nie[1, *], Dan H. Shugar[2], Jida Wang[3], Qian Deng[1, 4], Huayong Chen[1],

5 Jianrong Fan[1]

7 [1]Institute of Mountain Hazards and Environment, Chinese Academy of Sciences, Chengdu,

8 China

9 [2]Water, Sediment, Hazards, and Earth-surface Dynamics (waterSHED) Lab, Department of

10 Geoscience, University of Calgary, Alberta, T2N 1N4, Canada

11 [3]Department of Geography and Geospatial Sciences, Kansas State University, Manhattan,
12 Kansas 66506, USA

13 [4]University of Chinese Academy of Sciences, Beijing 100190, China
14
15
16
17 [*]Corresponding author, nieyong@imde.ac.cn
18

Abstract. The China-Pakistan Economic Corridor (CPEC) is one of the flagship projects of the One Belt One Road Initiative, which faces threats from water shortage and mountain disasters in the high-elevation region, such as glacial lake outburst floods (GLOFs). An up-to-date high-quality glacial lake dataset with parameters such as lake area, volume and type, which is fundamental to water resource and flood risk assessments, and predicting glacier-lake evolutions, is still largely absent for the entire CPEC. This study describes a glacial lake dataset for the CPEC using a threshold-based mapping method associated with rigorous visual inspection workflows. This dataset includes (1) multi-temporal inventories for 1990, 2000, and 2020 produced from 30 m resolution Landsat images, and (2) a glacial lake inventory for the year 2020 at 10 m resolution produced from Sentinel-2 images. The results show that, in 2020, 2234 lakes were derived from the Landsat images, covering a total area of 86.31 ± 14.98 km^2 with a minimum mapping unit of 5 pixels (4500 m^2), whereas 7560 glacial lakes were derived from the Sentinel-2 images with a total area of 103.70 ± 8.45 km^2 with a minimum mapping unit of 5 pixels (500 m^2). The discrepancy shows that Sentinel-2 is able to detect a significant quantity of smaller lakes than Landsat due to its finer spatial resolution. Glacial lake data in 2020 was validated by Google Earth-derived lake boundaries with a median ($\pm$standard deviation) difference of 7.66 ± 4.96 % for Landsat-derived product and 4.46 ± 4.62 % for Sentinel-derived product. The total number and area of glacial lakes from consistent 30 m resolution Landsat images remain relatively stable despite a slight increase from 1990 to 2020. A range of critical attributes have been generated in the dataset, including lake types and mapping uncertainty estimated by an improved Hanshaw's equation. This comprehensive glacial lake dataset has potential to be widely applied in studies on water resource assessment, glacial lake-related hazards, glacier-lake interactions, and is freely available at https://doi.org/10.12380/Glaci.msdc.000001 (Lesi et al., 2022).

1 Introduction

Glaciers in High-mountain Asia (HMA) play a crucial role in regulating climate, supporting ecosystems, modulating the release of freshwater into rivers, and sustaining municipal water supplies (Wang et al., 2019; Viviroli et al., 2020), agricultural irrigation, and hydropower generation (Pritchard, 2019; Nie et al., 2021). Most HMA glaciers are losing mass in the context of climate change (Brun et al., 2017; Maurer et al., 2019; Shean et al., 2020; Bhattacharya et al., 2021), therefore, unsustainable glacier melt and the passing of peak water are reducing the hydrological role of glaciers (Huss and Hock, 2018) and impacting downstream ecosystem services, agriculture, hydropower and other socioeconomic values (Carrivick and Tweed, 2016; Nie et al., 2021). The present and future glacier changes not only impact water supply for downstream area but also alter the frequency and intensity of glacier-related hazards, such as glacier lake outburst floods (GLOFs) (Nie et al., 2018; Rounce et al., 2020; Zheng et al., 2021), and rock and ice avalanches (Shugar et al., 2021). Global glacial lake number and total area both increased between 1990 and 2018 in response to glacier retreat and climate change (Shugar et al., 2020), affecting the allocation of freshwater resource. The Indus is globally the most important and vulnerable water tower unit where glaciers, lakes and reservoir storage contribute about two-thirds of the water supply (Immerzeel et al., 2020). Ice-marginal lakes store ~1% of total ice discharge in Greenland and accelerate lake-terminating ice velocity by ~25% (Carrivick et al., 2022). An increasing

63   frequency and risk of GLOFs (Nie et al., 2021; Zheng et al., 2021) is threatening Asian
64   population and infrastructures in the mountain ranges, such as the China-Pakistan Economic
65   Corridor (CPEC), as a flagship component of One Belt One Road Initiative (Battamo et al.,
66   2021; Li et al., 2021). The northern section of the CPEC passes through Pamir, Karakoram,
67   Hindu Kush and Himalaya mountains where droughts and glacier-related hazards are frequent
68   and severe (Hewitt, 2014; Bhambri et al., 2019; Pritchard, 2019), threatening local people,
69   the existing, under-construction and planned infrastructures, such as highways, hydropower
70   plants and railways. Understanding the risk posed by water shortage and glacier-related
71   hazards is a critical step to sustainable development for the CPEC.
72   Glacial lake inventories with a range of attributes benefit water resource assessment and
73   disaster risk assessment related to glacial lake (Wang et al., 2020; Carrivick et al., 2022), and
74   contribute to predicting glacier-lake evolution and cryosphere-hydrosphere interactions under
75   climate change (Nie et al., 2017; Brun et al., 2019; Maurer et al., 2019; Carrivick et al., 2020;
76   Liu et al., 2020). Remote sensing is the most viable way to map glacial lakes and detect their
77   spatio-temporal changes in the high-elevation zones where in situ accessibility is extremely
78   low (Huggel et al., 2002; Quincey et al., 2007). Studies in glacial lake inventories using
79   satellite observations have been heavily conducted at regional scales recently, such as in the
80   Tibetan Plateau (Zhang et al., 2015), the Himalaya (Gardelle et al., 2011; Nie et al., 2017),
81   the HMA (Wang et al., 2020; Chen et al., 2021), the Tien Shan (Wang et al., 2013), the
82   Alaska (Rick et al., 2022), the Greenland (How et al., 2021) and the northern Pakistan
83   (Ashraf et al., 2017). However, the latest glacial lake mapping in 2020 is still absent along the
84   CPEC. Among existing studies, Landsat archival images are the most widely used due to their
85   multi-decadal record of earth surface observations, reasonably high spatial resolution (30 m),
86   and publicly available distribution (Roy et al., 2014). Freely available Sentinel-2 satellite
87   images show a better potential than Landsat in glacial lake mapping and inventories due to
88   their higher spatial resolution (10 m) and a global coverage, but have only been available
89   since late 2015 (Williamson et al., 2018; Paul et al., 2020). Glacial lake inventories using
90   Sentinel-2 images are relatively scarce at regional scales, and studies of the latest glacial lake
91   mapping as well as comparisons of glacial lake dataset derived from Sentinel-2 and Landsat
92   observations are still lacking.
93   Discrepancies between various glacial lake inventories (Zhang et al., 2015; Shugar et al.,
94   2020; Wang et al., 2020; Chen et al., 2021; How et al., 2021) result from differences in
95   mapping methods, minimum mapping units, definition of glacial lakes, time periods, data
96   sources and other factors. For example, manual vectorization method was widely adopted at
97   the earlier stage for its high accuracy. However, it is time-consuming associated with high
98   labor intensity and is only practical at regional scales (Zhang et al., 2015; Wang et al., 2020).
99   Automated and semi-automated lake mapping methods, such as multi-spectral index
100   classification (Gardelle et al., 2011; Nie et al., 2017; Zhang et al., 2018; How et al., 2021),
101   have been developed to improve the efficiency of glacial lake inventories using optical
102   images, although manual modification is often unavoidable to assure the quality of lake data
103   impacted by cloud cover, mountain shadows, seasonal snow cover and frozen lake surfaces
104   (Sheng et al., 2016; Wang et al., 2017, 2018). Backscatter images from Synthetic Aperture
105   Radar (SAR) (Wangchuk and Bolch, 2020; How et al., 2021) were used to remove the impact
106   of cloud cover for lake mapping. Besides, other approaches such as hydrological sink

107   detection using DEM (How et al., 2021) and land surface temperature-based detection
108   method (Zhao et al., 2020) were also used for lake inventories. Different classification
109   methods impact the results of lake mapping and monitoring. So far, we are lacking a unified
110   standard for the classification system of glacial lakes (Yao et al., 2018). Existing
111   classification systems are generally used for their individual research purposes, mainly based
112   on the relative positions of glacial lakes and glaciers, the supply conditions of glaciers, and
113   the attributes of dams. In addition to different classification standards, the same type of
114   glacial lakes may also have different names given by different scholars. For example, ice-
115   marginal (Carrivick and Quincey, 2014; Carrivick et al., 2020), ice-contact (Carrivick and
116   Tweed, 2013) and proglacial (Nie et al., 2017) lakes all represent glacial lakes sharing the
117   boundary with glaciers. Glacier lakes in currently available datasets have been traditionally
118   categorized by their spatial relationship with upstream glaciers (Gardelle et al., 2011; Wang
119   et al., 2020; Chen et al., 2021), and classification attributes considering the formation
120   mechanism and the properties of dams are rare or incomplete in the CPEC (Yao et al., 2018;
121   Li et al., 2020). Dam type classification of glacial lakes provides a crucial attribute for
122   glacier-lake interactions and risk assessment (Emmer and Cuřín, 2021). Therefore, an up-to-
123   date glacial lake dataset with critical, quality-assured parameters (e.g. lake area, volume and
124   type) is necessary.
125   This study aims to (1) present an up-to-date glacial lake dataset in the CPEC in 2020 using
126   both Landsat 8 and Sentinel-2 images to accurately document its detailed lake distribution;
127   (2) present two historical glacial lake datasets for the CPEC to show extent in 1990 and 2000
128   using consistent 30-m Landsat images to reveal glacial lake changes at three time periods
129   (1990, 2000 and 2020); and (3) generate a range of critical attributes for glacial lake
130   inventories to benefit studies on water resource evaluation, risk assessment of GLOFs, glacier
131   –lake evolution modeling in the HMA.
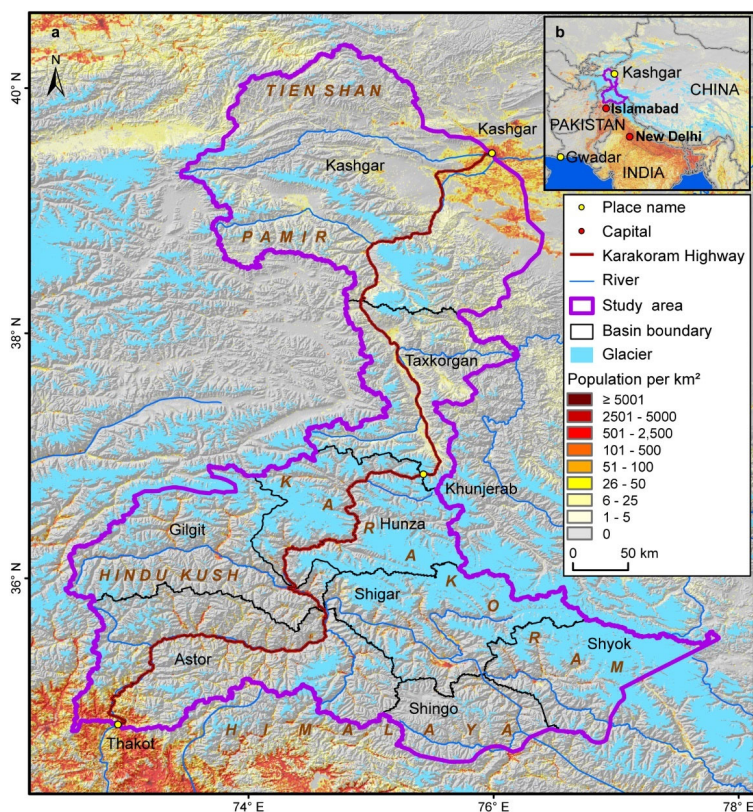
2 Study area

Figure 1. Location of the study area associated with distribution of glaciers (RGI Consortium, 2017), mountains, basins and population (Rose et al., 2021) (a), and its location within the CPCE (b).

The northern part of the CPEC is selected as the study area (Figure 1Figure 1). The CPCE, originating from Kashgar of the Xinjiang Uygur Autonomous region, China and extending to Gwadar Port, Pakistan (Ullah et al., 2019; Yao et al., 2020), is connecting China and Pakistan via the only Karakoram Highway. The study area covers all the drainage basins along Karakoram Highway starting from Kashgar and ending at Thakot, with a total area of ~125,000 km^2. The upper Indus basins beyond the Pakistani-administrated border are excluded in this study due to spatial coverage of the CPCE. The entire study area is divided into eight sub-basins, covering most of the Karakoram with the highest elevation up to 8611 m, western Himalaya and Tien Shan, eastern Hindu Kush and Pamir Mountains. The 9710 glaciers in the study area cover a total area of 17,447 km^2 and nearly 60% of glaciers are distributed in the Karakoram (5818 glaciers with a total area of 14,067.52 km^2) (RGI Consortium, 2017). Most glaciers in the western Himalaya and eastern Hindu Kush are losing mass in the context of

149 climate change (Kääb et al., 2012; Yao et al., 2012; Brun et al., 2017; Shean et al., 2020;
150 Hugonnet et al., 2021), whereas the glaciers in the eastern Karakoram and Pamir have shown
151 unusually little changes, including unchanged, retreated, advanced and surged glaciers (Hewitt,
152 2005; Kääb et al., 2012; Bolch et al., 2017; Brun et al., 2017; Shean et al., 2020; Nie et al.,
153 2021). The spatially heterogeneous distribution and changes of glaciers are primarily explained
154 as a result of differences in the dominant precipitation-bearing atmospheric circulation patterns
155 that include the winter westerlies the Indian summer monsoon, their changing trends and their
156 interactions with local extreme topography (Yao et al., 2012; Azam et al., 2021; Nie et al.,
157 2021).

3 Data sources

159 Both Landsat and Sentinel-2 images have been employed to map glacial lakes between 1990
160 and 2020 in the CPEC (Figure 2Figure 2). A total number of 71 Landsat Thematic Mapper
161 (TM), Thematic Mapper Plus (ETM+) and Landsat 8 Operational Land Imager (OLI) images
162 with a consistent spatial resolution of 30 m were downloaded from the United States
163 Geological Survey Global Visualization Viewer (GloVis, https://glovis.usgs.gov/) to be used
164 to create glacial lake inventories in 1990, 2000 and 2020. High-quality Landsat-5 images
165 around 2010 are insufficient to cover the entire study area, so we were unable to map lakes in
166 2010 due to Landsat-7's scan-line corrector errors and significant cloud covers. In addition,
167 39 Sentinel-2 images (23 scenes in 2020) were downloaded from Copernicus Open Access
168 Hub (https://scihub.copernicus.eu/) to produce the 10-m resolution glacial lake inventory in
169 2020. All images used in this study have been orthorectified before download, but we still
170 find that one Sentinel-2 image was not well matched with Landsat images, leading to the
171 discrepancy between the two glacial lake datasets. We manually georeferenced the shifted
172 image to minimize the difference between Sentinel and Landsat derived glacial lakes.
173 Cloud and snow covers heavily affect the usability of optical satellite images (Wulder et
174 al., 2019) and their availability in the entire study area, so we took advantage of the images
175 acquired before and after each of the baseline years 1990, 2000 and 2020 to construct the
176 glacial lake inventories. Only 4 images in 1990 (the largest covering the study area), 16
177 images in 2000 and 23 images in 2020 were used for matching baseline year. Spatially, high-
178 quality images in given baseline years were preferentially chosen, or we selected one or more
179 alternative images acquired in adjacent years to delineate glacial lakes by removing the effect
180 of cloud and snow covers. To minimize the impact of intra-annual changes of glacial lakes,
181 most of used images (82% for Sentinel-2 and 75% for Landsat) were acquired from August to
182 October in the given baseline year with cloud coverage of <20% for each image. For some
183 specific scenes where cloud cover exceeded the threshold of 20%, we selected more than one
184 image to remedy the effect of cloud contamination (Nie et al., 2010, 2017; Jiang et al., 2018).
185 Other datasets used include the Randolph Glacier Inventory version 6.0 (Pfeffer et al.,
186 2014; RGI Consortium, 2017) and the Glacier Area Mapping for Discharge from the Asian
187 Mountains (GAMDAM) glacier inventory (Sakai, 2019). These two glacier datasets were
188 used to determine glacial lake types, such as ice-contact, ice-dammed and unconnected-
189 glacier-fed lakes. The Shuttle Radar Topography Mission Digital Elevation Model (SRTM
190 DEM) at a 1-arc second (30 m) resolution (Jarvis et al., 2008) was employed to extract the
191 altitudinal characteristics of the glacial lakes. The absolute vertical accuracy of the SRTM

带格式的: 字体: (中文) 宋体, 非加粗

192   DEM is 16 m (90%) (Rabus et al., 2003; Farr et al., 2007). We also applied other published
193   glacial lake datasets for comparative analysis. They include the glacial lake inventories of
194   HMA in 1990 and 2018 downloaded from http://doi.org/10.12072/casnw.064.2019.db (Wang
195   et al., 2020), the Third Pole region in 1990, 2000 and 2010 publicly shared at
196   http://en.tpedatabase.cn/ (Zhang et al., 2015), the Tibet Plateau from 2008 to 2017 accessed at
197   https://doi.org/10.5281/zenodo.3700282 (Chen et al., 2021), and the entire world in 1990,
198   2000 and 2015 provided at https://nsidc.org/data /HMA_ GLI/versions/1 (Shugar et al.,
199   2020). In addition, field survey data collected between 2017 and 2018 were also used to assist
200   in lake mapping and glacial lake type classification.

201
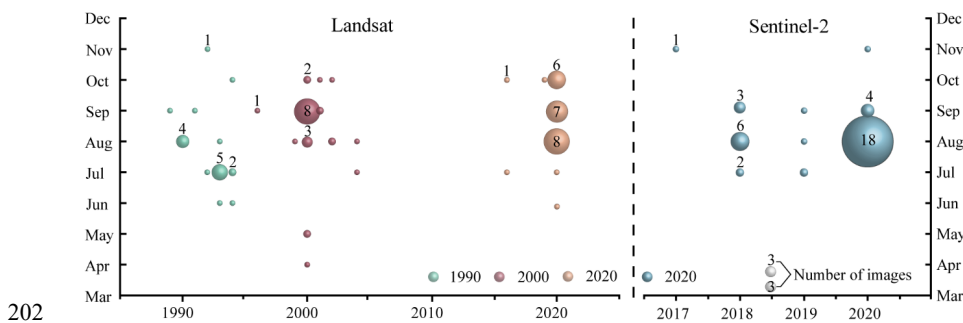
202

Figure 2. Acquisition years and months of Landsat and Sentinel-2 images selected for glacial lake
inventories. The bubble size indicates the available high-quality image number.

4 Glacial lake inventory methods

4.1 Definition of glacial lakes

207   We consider a glacial lake as one that formed as a result of modern or ancient glaciation.
208   Contemporary glacial lakes are easily recognized using a combination of glacier inventories
209   and remote sensing images. Ancient glacial lakes can be identified from periglacial
210   geomorphological characteristics, including moraine remnants and U-shaped valleys that are
211   discernible from satellite observations (Post and Mayo, 1971; Westoby et al., 2014; Nie et al.,
212   2018; Martín et al., 2021). A 10-km buffering distance of RGI 6.0 glacier boundaries that has
213   been widely used in previous studies (Zhang et al., 2015; Wang et al., 2020), was created to
214   help mapping glacial lakes. A few glacial lakes in the study area (a total of 84 lakes for
215   Sentinel-2 dataset and 55 lakes for Landsat dataset in 2020) beyond the buffering zone,
216   located near buffering boundaries, were intentionally included due to clear evidence of
217   glaciation (Figure 3Figure 3). Landslide-dammed lakes (Chen et al., 2017) in the buffering
218   zone were excluded in our inventories because of their irrelevance to glaciation. All glacial
219   lakes in the study area were mapped according to our definition. We were able to implement
220   this definition by carefully leveraging the spectral properties of glacial lakes and the
221   periglacial geomorphological features that are often evident in remote sensing images (see
222   more in sections 4.3 and 4.4).

223

带格式的: 字体: 非加粗
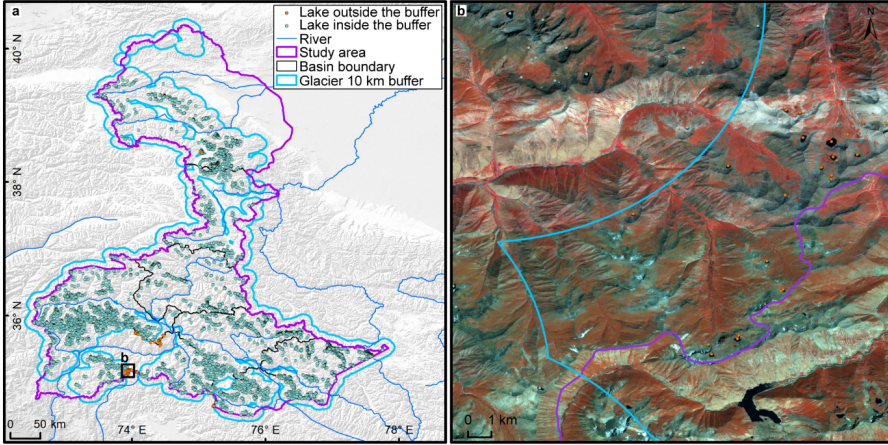
224

225 **Figure 3.** The 10-km buffer zone of RGI 6.0 glacier boundaries (a) and Sentinel-derived glacial lakes
226 located near buffering boundary within the study area (b).

227

228 4.2 Interactive lake mapping

229 A human-interactive and semi-automated lake mapping method (Wang et al., 2014; Nie et al.,
230 2017, 2020) was adopted to accurately extract glacial lake extents using Landsat and
231 Sentinel-2 images, based on the Normalized Difference Water Index (NDWI) (Mcfeeters,
232 1996). The NDWI uses the green and near infrared bands and is calculated by the following
233 equation:

234 $$NDWI = \frac{Band_{Green} - Band_{NIR}}{Band_{Green} + Band_{NIR}} \qquad (1)$$

235 where the green band and near infrared band were provided by both Landsat and Sentinel
236 multispectral images.
237   Specifically, the method calculated the NDWI histogram based on the pixels with each
238 user-defined and manually-drawn region of interest. The NDWI threshold that separates lake
239 surface from land was interactively determined by screening the NDWI histogram against the
240 lake region in the imagery (Wang et al., 2014; Nie et al., 2020). This way, the determined
241 NDWI threshold can be well-tuned to adapt various spectral conditions of the studied glacier
242 lakes. The raster lake extents segmented by the thresholds were then automatically converted
243 to vector polygons. We first completed the glacial lake inventory in 2020 using this
244 interactive mapping method, and the 2020 inventory was then used as a reference to facilitate
245 the lake mapping for other periods.
246   The minimum mapping unit (MMU) was set to 5 pixels for both Landsat (0.0045 km^2) and
247 Sentinel-2 images (0.0005 km^2) in this study. MMU determines the total number and area of
248 glacial lakes in the dataset, and varies in the previous studies, such as 3 pixels (Zhang et al.,
249 2015), 6 pixels (Wang et al., 2020), or 9 pixels (Chen et al., 2021) for a regional scale, or 55
250 pixels (Shugar et al., 2020) for a global scale. While a smaller threshold leads to a large
251 quantity of lakes mapped, it also generates larger mapping noises or uncertainties.

252 Considering this signal-noise balance and our focus on identifying prominent glacier lake
253 dynamics in the study area, we opted to use 5 pixels as the MMU for both Landsat and
254 Sentinel-2 images.
255   Several procedures were taken to assure the quality assurance and quality control for lake
256 mapping, including 1) visual inspection and modification using the threshold-based mapping
257 method for each lake according to Landsat, Sentinel-2 and Google Earth high-resolution
258 images overlaying preliminarily lake boundary extraction at the given time period; 2) time
259 series check for Landsat-derived glacial lake datasets from 1990 and 2020, and cross-check
260 between Landsat and Sentinel-2-derived lake dataset in 2020 to reduce errors of omission and
261 commission; 3) topological validation of glacial lake mapping, such as repeated removal,
262 elimination of small sliver polygons; and 4) logical check for lake types between two
263 classification systems of glacial lakes. False lake extents resulting from cloud or snow cover,
264 lake ice, and topographic shadows (Nie et al., 2017, 2020) were modified using previous
265 semi-automated mapping method based on alternative images acquired in adjacent years.
266 Those procedures were time-consuming, but helped to minimize the effect of cloud and snow
267 covers, lake mapping errors, and to maximize the quality of the produced lake product and
268 the derived glacial lake changes.

269 4.3 Classification of glacial lakes

270 Two glacial lake classification systems (GLCS) have been established based on relationship
271 of interaction between glacial lakes and glaciers as well as lake formation mechanism and
272 dam material properties. In the first GLCS (GLCS1), glacial lakes were classified into four
273 types based on their spatial relationship to upstream glaciers: supraglacial, ice-contact,
274 unconnected-glacier-fed lakes, and non-glacier-fed lakes according to Gardelle et al. (2011)
275 and Carrivick et al. (2013). Alternatively, combining the formation mechanism of glacial
276 lakes and the properties of natural dam features, glacial lakes were classified into five
277 categories (herein named GLCS2) modified from Yao's classification system (2018):
278 supraglacial, end-moraine-dammed, lateral-moraine-dammed, glacial-erosion lakes and ice-
279 dammed lakes. Subglacial lakes were excluded due to the mapping challenge from spectral
280 satellite images alone. Characterization and examples for each type are provided in Table
281 1Table 1 and Table 2Table 2. Individual glacial lakes were categorized to the specific types
282 for each GLCS according to available glacier inventory data, geomorphological and spectral
283 characteristics interpreted from Landsat, Sentinel and Google Earth images. The synergy of
284 these two GLCSs is beneficial to predicting glacier-lake evolutions and providing
285 fundamental data for water resource and glacial lake disaster risk assessment.
286

287
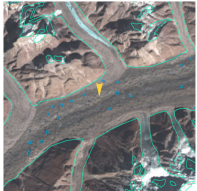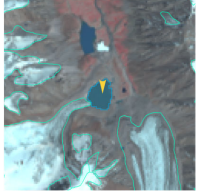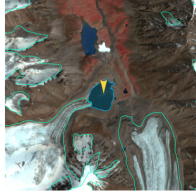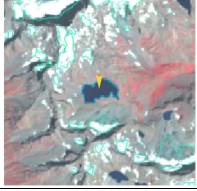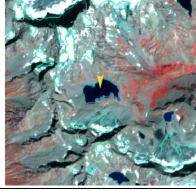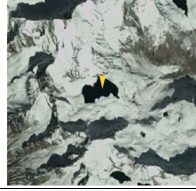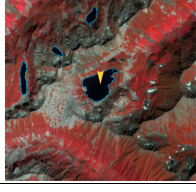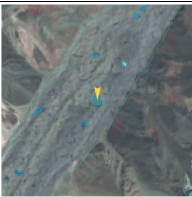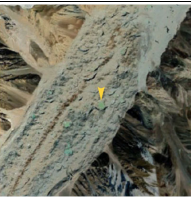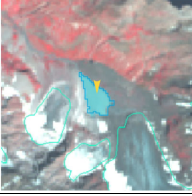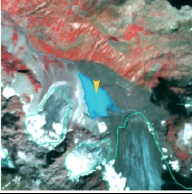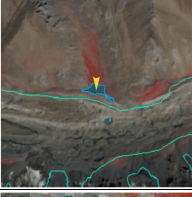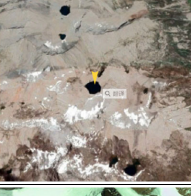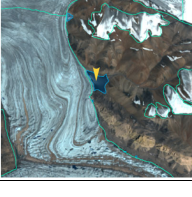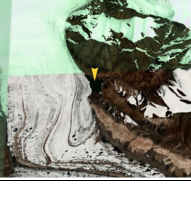
Table 1. Classification system of glacial lake types (GLCS1) according to the relationship between glacial lakes and glaciers (© Google Earth 2019). Glacier outlines are from RGI 6.0 (RGI Consortium, 2017), and the yellow marker represents target lake.

Lake types	Characteristics	Landsat	Sentinel-2	Google Earth
Supraglacial	Lakes formed on the surface of glaciers, generally dammed by ice and thin debris. Case location: 35°43'49.74" N 76°13'53.88" E			
Ice-contact	Lakes dammed by moraine, ice or bedrock, supplied by glacial meltwater and shared boundary with glaciers. Case location: 39°09'32.40" N 73°43'12.00" E			
Unconnected-glacier-fed	Lakes currently supplied by upstream glacial meltwater but disconnected with glaciers. Case location: 35°47'60.00" N 72°55'15.60" E			
Non-glacier-fed	Lakes formed by glaciology, dammed by moraine or bed rock, and currently not supplied by glacial meltwater. Case location: 34°50'39.99" N 74°48'29.31" E			

291

Table 2. Classification system of glacial lake types (GLCS2) according to the formation mechanism of glacial lakes and dam material properties (© Google Earth 2019). Glacier outlines from RGI 6.0 (RGI Consortium, 2017), and the yellow marker represents target lake.

Lake types	Characteristics	Landsat	Sentinel-2	Google Earth
Supraglacial	Lakes formed on the surface of glaciers, generally dammed by ice and thin debris. Case location: 36°46'7.39" N 74°20'7.59" E			
End-moraine-dammed	Lakes formed behind moraines as a result of glacier retreat and downwasting. Case location: 35°42'50.40" N 73°09'57.60" E			
Lateral-moraine-dammed	Lakes formed behind lateral glacial moraine ridges and dammed by debris, different from ice-dammed glacial lake. Case location: 38°28'45.62" N 75°20'52.30" E			
Glacial-erosion	Lakes formed in depressions created by glacial over-deepening. Bedrock dam dominates, partially superimposed by top moraine in rugged terrain. Dams are unclear in the satellite images. Case location: 35°55'55.56" N 73°38'20.13" E			
Ice-dammed	Lakes formed behind glaciers, dammed by glacier ices (partially covered by debris on the top). Case location: 35°28'31.32" N 77°30'46.81" E			

4.4 Attributes of glacial lake data

A total of 18 attribute fields were input into our glacial lake datasets (Table 3~~Table 3~~). They include lake location (longitude and latitude), lake elevation (centroid elevation), orbital number of the image source, image acquisition date, lake area, lake perimeter, lake types of the two GLCSs, mapping uncertainty, lake water volume and the country, sub-basin, and mountain range associated with the lake. Amongst the attributes, lake location was calculated based on

302 the centroid of each glacial lake polygon associated with the DEM, N represents northing and
303 E represents easting. Orbital number of the image source was filled with the corresponding
304 satellite image, with the codes expressed as "PxxxRxxx" or "Txxxxx", where P and R indicate
305 the path and row for Landsat image and T represents the tile of Sentinel-2 image associated
306 with 5 digit code of military grid reference system. SceneID indicated identifying information
307 of image source for Landsat or Sentinel-2, consisted of the orbital number, sensor ID and
308 acquisition date (YYYYMMDD) for Landsat image, or the orbital number and acquisition date
309 (YYYYMMDD) for Sentinel-2 image. Area and perimeter were automatically calculated based
310 on glacial lake extents. Lake water volume was estimated by area-volume empirical equation
311 (Cook and Quincey, 2015). Lake types were attributed using the characterization and
312 interpretation marks described in Section 4.3. Mapping uncertainty was estimated using our
313 modified equation which will be introduced in section 4.5 and appendix tutorial. Located
314 country, sub-basin and mountain range of each glacial lake was identified by overlapping the
315 geographic boundaries of countries, basins and mountain ranges.
316
317 **Table 3.** Attributes of glacial lake dataset.

Field Name	Type	Description	Note
FID or OBJECTID	Object ID	Unique code of glacial lake	Number
Shape	Geometry	Feature type of glacial lake	Polygon
Latitude	String	Latitude of the centroid of glacial lake polygon	Degree minute second
Longitude	String	Longitude of the centroid of glacial lake polygon	Degree minute second
Elevation	Double	Elevation of the centroid of glacial lake polygon	Unit: meter above sea level
SceneID	String	Scene ID of image source for Landsat or Sentinel-2	PxxxRxxx_xxxDYYYYMMDD or Txxxxx_YYYYMMDD
ACQDATE	String	Acquisition date of source image	YYYYMMDD
GLCS1	String	The first classification system of glacial lakes based on relationship of interaction between glacial lakes and glaciers	Supraglacial, Ice-contact, Unconnected-glacier-fed, None-glacier-fed

Field Name	Type	Description	Note
GLCS2	String	The second classification system of glacial lakes based on lake formation mechanism and dam material properties	Supraglacial, End-moraine-dammed, Lateral-moraine-dammed, Glacial-erosion and Ice-dammed
Basin	String	Basin name where glacial lake locates in	
Mountain	String	Mountain name where glacial lake locates in	
Country	String	Country name where glacial lake locates in	
Perimeter	Double	Perimeter of glacial lake boundary	Unit: meter
Area	Double	Area of glacial lake coverage	Unit: square meter
AreaUncer	Double	Area uncertainty of glacial lake mapping estimated based on modified Hanshaw's equation (2014)	Unit: square meter
Operator	String	Operator of glacial lake dataset	Muchu, Lesi
Examiner	String	Examiner of glacial lake dataset	Yong, Nie
Volume	Double	Water volume of glacial lake estimated by area-volume empirical equation	Unit: cubic meter

318

319 ## 4.5 Error and uncertainty assessment

320 ### 4.5.1 Improved uncertainty estimating method

321 We modified Hanshaw's (2014) equation that had been used to calculate lake-area mapping
322 uncertainty. Lake perimeter and displacement error are widely used to estimate the
323 uncertainty of glacier and lake mapping from satellite observation (Carrick and Quincey,
324 2014; Hanshaw and Bookhagen, 2014; Wang et al., 2020). Hanshaw and Bookhagen (2014)
325 proposed an equation to calculate the error of area measurement by the number of edge pixels
326 of the lake boundary multiplied by half of a single pixel area. The number of edge pixels is
327 simply calculated by the perimeter divided by the grid size. The equation is expressed as
328 below:

329
$$Error(1\sigma) = \frac{P}{G} \times 0.6872 \times \frac{G^2}{2} \tag{2}$$

330
$$D = \frac{Error(1\sigma)}{A} \times 100\% \tag{3}$$

331 Where G is the cell size of the remote sensing imagery (10 m for Sentinel-2 image and 30 m
332 for Landsat image). P is the perimeter of individual glacial lake (m), and the coefficient of
333 0.6872 (1σ), which means nearly 69% of the edge pixels are subject to errors (Hanshaw and
334 Bookhagen, 2014), was chosen assuming that area measurement errors follow a Gaussian
335 distribution. Relative error (D) was calculated by equation 3, in which A is the area of an
336 individual glacial lake.
337   In the original equation 2, the number of edge pixels varies by the shape of lake and is
338 indicated by $\frac{P}{G}$. However, the pixels in the corner are double counted (Figure 4Figure 4). The
339 total number of repeatedly calculated edge pixels equals the number of inner nodes.
340 Therefore, we adjusted the calculation of the actual number of edge pixels as the maximum of
341 edge pixels ($\frac{P}{G}$) subtracting the number of inner nodes. Accordingly, the equation of
342 uncertainty estimation for lake mapping is modified as below:

343
$$Error(1\sigma) = (\frac{P}{G} - N_{Inner}) \times 0.6872 \times \frac{G^2}{2} \tag{4}$$

344 Where N_{Inner} is the number of inner nodes (inflection points) of each lake. The modified
345 equation is also suitable for lakes with islands (as illustrated in Figure 4Figure 4b).
346   For polygons without islands (Figure 4Figure 4a), use the following equation:

347
$$N_{Inner} = (\frac{N_{Total}-4-1}{2}) \tag{5}$$

348 N_{Total} is the total number of nodes, including both the outer and inner. N_{Total} is calculated
349 by the "Field Calculator" in ArcGIS, in some cases, it is necessary to remove the redundant
350 nodes before calculating the total number of nodes (See the Appendix for more details). An
351 inner node is a polygon vertex where the interior angle surrounding it is greater than 180
352 degrees. An outer node is the opposite of the inner node, where the interior angle is less than
353 180 degrees. We found that the outer nodes are usually four more than the inner nodes in our

glacial lake dataset. The total nodes in ArcGIS contain one overlapping node to close the polygon, meaning the endpoint is also the startpoint. This extra count was deleted in the calculation (equation 5).

For polygons with island (Figure 4Figure 4b) use the following equation:

$$N_{Inner} = (\frac{N_{Total}-(N_{Island}+1)\times 5}{2}) \tag{6}$$

N_{Island} is the number of islands within each polygon. A calculation method of N_{Island} is given in the Appendix.

| Lake | Non-water pixel | • Inner node |
| Edge pixel | Double counted pixel | Lake boundary |
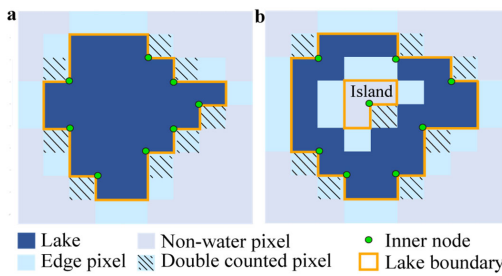
Figure 4. Sketch of estimating the actual edge pixels for uncertainty calculation of individual glacial lake (with (a) and without islands (b)).

4.5.2 Validation of glacial lake mapping

A total of 89 glacial lakes were selected by stratified random sampling and manually digitized based on the Google Earth images in circa 2020 with a spatial resolution of ～2 m acquired from WorldView, GeoEye, Pleiades etc. satellites to further validate the absolute error of our glacial lake products in 2020 due to lacking of field measurements for glacial lakes in the study area. During the sampling, we set a minimum lake area to be 4500 m^2 and a relative difference between Landsat- and Sentinel-derived lake areas less than 18% (nearly equaling to the average relative error of ±17.36% for Landsat lake mapping) in order to minimize the effect of lake changes from multi-temporal satellite observations in circa 2020. The 89 sample lakes range from 0.005 km^2 to 0.802 km^2 with a median (standard deviation) size of 0.047±0.134 km^2 and a total area of 8.033 km^2 for Landsat-derived dataset, and range from 0.005 km^2 to 0.849 km^2 with a median (standard deviation) size of 0.045±0.144 km^2 and a total area of 8.447 km^2 for Sentinel-derived dataset.

5 Results

5.1 Glacier lake distribution and changes observed from Landsat

We mapped 2,234 glacial lakes for 2020 across the studied CPEC from Landsat-8 images, with a total area of 86.31±14.98 km^2 (Figure 5Figure 5a and b). Unconnected-glacier-fed

lakes are dominant in the first classification system, followed by non-glacier-fed lakes (Figure 6Figure 6) whereas glacial-erosion lakes dominate at both number (1478) and area (57.02 km^2) in the second classification system (Figure 7Figure 7), followed by end-moraine-dammed lakes and supraglacial lakes. Among the classified lakes, 137 are ice-contact lakes and cover an area of 5.56 km^2, implying a higher mean size of ice-contact lakes than supraglacial lakes.
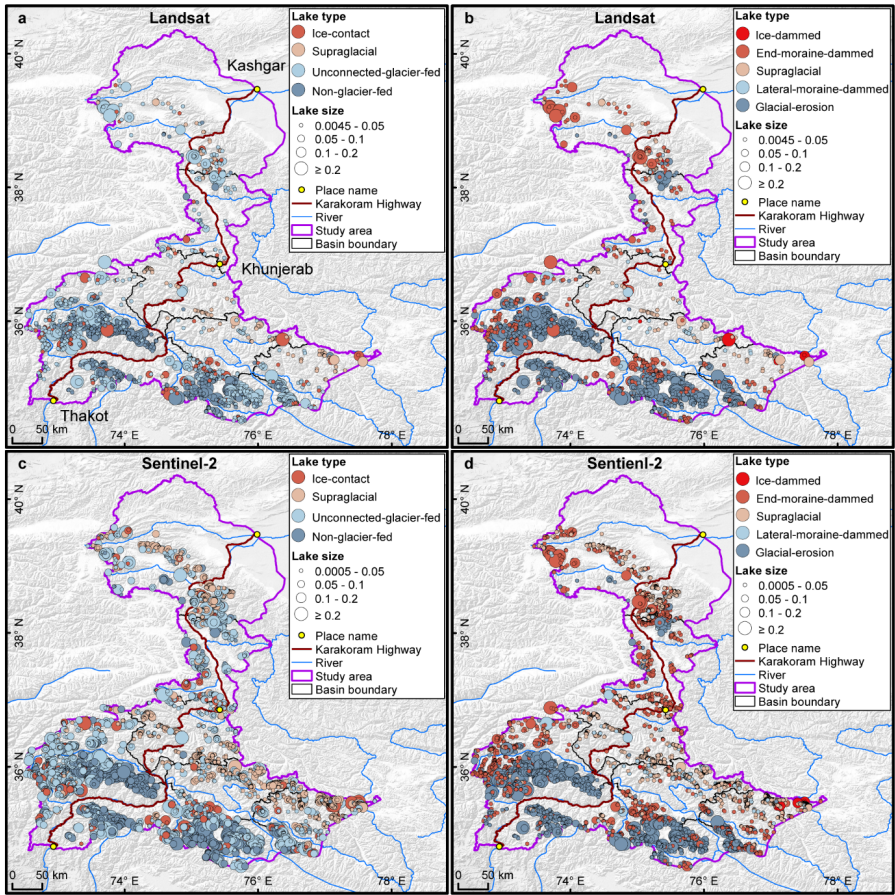
Figure 5. Distribution of glacial lakes in 2020 extracted from Landsat (a, b) and Sentinel-2 (c, d) images. Panels a and c are classified by GLCS1, and GLCS2 for sub-graph b and d.

395
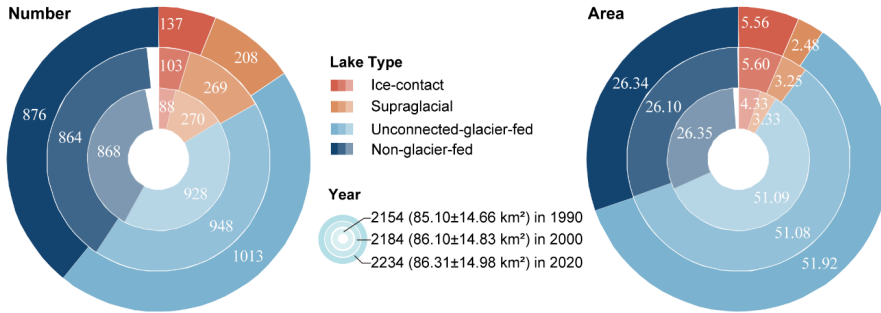
Figure 6. Number and area of different types of glacial lakes classified based on the condition of glacier supply in the study area (GLCS 1). The outermost ring represents glacial lake data in 2020, middle ring for 2000 and innermost ring for 1990. Lake number and area in 2020 were selected as reference, meaning a concept of "100 %" for a complete ring. Labeled values are scaled in degrees rather the radius of rings.

400

401
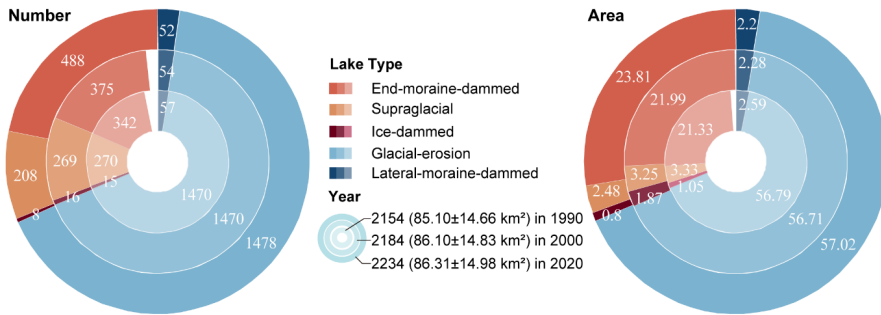
Figure 7. Number and area of different types of glacial lakes classified based on glaciation and nature of dam in the study area (GLCS 2). The outermost ring represents glacial lake data in 2020, middle ring for 2000 and innermost ring for 1990. Lake number and area in 2020 were selected as reference, meaning a concept of "100 %" for a complete ring. Labeled values are scaled in degrees rather the radius of rings.

406

The total number and area of glacial lakes in the study remain relatively stable with a slight increase between 1990 and 2020, and the changes in count and area among various types of glacial lakes vary substantially (Figure 6Figure 6 and Figure 7Figure 7). From 1990 to 2020, the total number of glacial lakes increased by 80 or 3.70%, while the area grew by 1.21 km^2 (or 1.42%). In GLCS1, unconnected-glacier-fed lakes have the largest increase in number, followed by ice-contact and non-glacier-fed lakes, whereas supraglacial lakes decreased by 62 in count. Ice-contact lakes expanded by 1.24 km^2 (equaling an increase of 26% in ice-contact lakes), contributed one third of the total area increase. Supraglacial lakes decreased by 0.85 km^2 in area whereas the areas of unconnected-glacier-fed and non-glacier-fed lakes remained stable as a result of disconnections from glaciers (Figure 6Figure 6). In GLCS2, end-moraine-dammed lakes increased by 2.48 km^2 and contributed most of the glacier lake area expansion, whereas supraglacial, ice-dammed and lateral-moraine-dammed

419 lakes decreased slightly in both number and area. Glacial-erosion lakes accounted for the
420 maximum percentage (about 66% for both count and area) in each time period and remained
421 stable (Figure 7~~Figure 7~~).

422 5.2 Glacier lake distribution observed from Sentinel-2

423 Sentinel-derived results shows that there are 7,560 glacial lakes (103.70±8.45 km^2) in 2020
424 across the entire CPEC ~~(Table 4)~~ under a MMU of 5 pixels (500 m^2). Compared with
425 Landsat-derived product, glacial lakes from Sentinel-2 have similar spatial distribution
426 characteristics (Figure 5~~Figure 5~~); meanwhile, a larger quantity of glacier lakes, with more
427 accurate boundaries and a greater total lake area, were generated from Sentinel-2 images
428 (Table 4). The smallest size class (0.0005-0.0045 km^2) contains the maximum lake number
429 (4,969) but the least lake area (7.73±2.62 km^2) ~~(Table 4)~~, which is not available in the
430 Landsat-derived lake data due to a coarser spatial resolution. In each size class, the overlap
431 ratios are greater than 85% in count and area, and there are also a higher number of larger
432 glacial lakes from Sentinel than that from Landsat images. The discrepancy is mainly
433 attributed to the inconsistency of spatial resolutions and image acquisition dates.
434
435 **Table 4.** Count and area of glacial lakes mapped from Sentinel-2 and Landsat images in 2020 ~~between~~ in
436 various size classes.

Lake size km^2	Glacial lakes from Sentinel-2 count (km^2)	Glacial lakes from Landsat count (km^2)	Overlap % (%)
0.0045-0.05	2182 (35.52±3.72)	1870 (31.47±9.57)	85.70 (88.60)
0.05-0.1	237 (16.37±0.89)	204 (14.07±2.18)	86.08 (85.95)
0.1-0.2	122 (16.88±0.68)	115 (15.91±1.83)	94.26 (94.25)
≥0.2	50 (27.20±0.54)	45 (24.86±1.40)	90.00 (91.40)
Total	~~7560~~2591 (95.97±5.83~~103.70±8.45~~)	2234 (86.31±14.98)	86.22 (89.93) ~~—~~

437 Note: Second column excludes 4969 (7.73±2.62) lakes in the 0.0005 to 0.0045 km^2 range. Overlap % (%) represent the ratios
438 between our Landsat-derived dataset and Sentinel-derived product in count and area, respectively~~the rates in count and area~~
439 ~~calculated by dividing Landsat-derived lake data by Sentinel-derived data in the same size class respectively~~.

6 Discussions

441 6.1 Uncertainty and error of lake mapping

442 The uncertainty estimated from our improved equation shows that the relative error of
443 individual glacial lake decreases when lake size increases or cell size of remote sensing
444 images reduces (Lyons et al., 2013; Carrivick and Quincey, 2014) (Figure 8~~Figure 8~~). Total
445 area errors of glacial lakes in study area are approximate ±14.98 km^2 and ±8.45 km^2 in 2020
446 for Landsat and Sentinel-2 dataset, respectively, and the average relative errors are ±17.36%
447 and ±8.15%. Generally, small lakes have greater relative errors. For example, the mean
448 relative error is 35.38% for Landsat derived glacial lakes between 0.0045 and 0.1 km^2 and
449 10.63% for glacial lakes greater than 0.1 km^2. The mean area error of Sentinel-derived glacial
450 lakes is almost one third of that extracted from Landsat images for glacial lakes of all or

451 specific size groups. Because the relative error was estimated as a function of satellite image
452 spatial resolution and lake perimeter, the calculated error for large lake is proportionally
453 smaller than that of small lake (Salerno et al., 2012) and the error for Landsat-derived lake is
454 naturally greater than that of Sentinel-derived lake at the same size group.
455
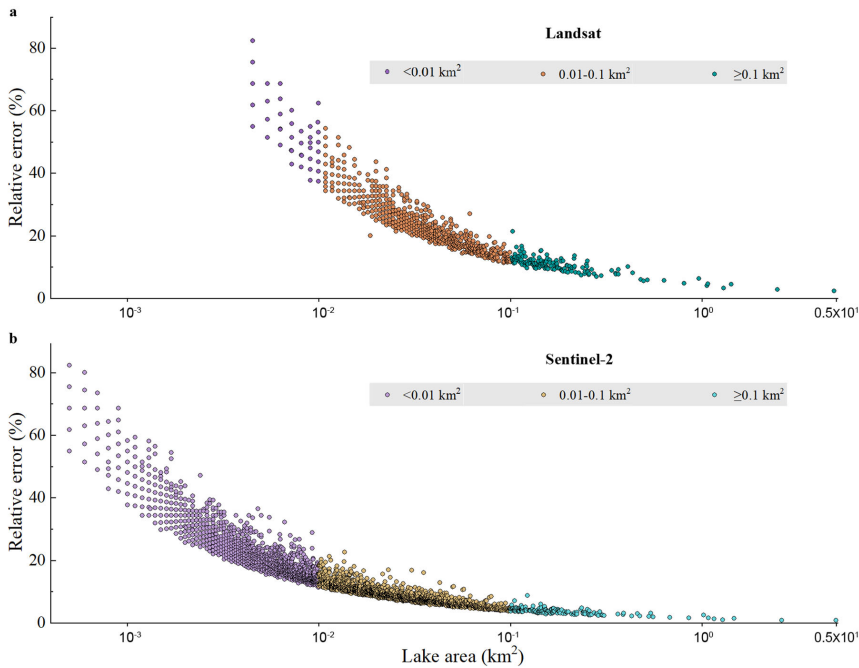
457 **Figure 8.** Estimated relative error for glacial lakes of all or specific size ranges in study area. Error
458 estimation is based on the modified equation and lake data extracted from Landsat (a) and Sentinel-2
459 images (b).
460

461 Our Landsat- and Sentinel-derived glacial lake dataset match well lake boundaries in Google
462 Earth higher resolution images (Figure 9Figure 9). The mean difference in area is 0.005 km^2
463 between Landsat and Google Earth derived lakes and 0.001 km^2 between Sentinel-2 and
464 Google Earth derived lakes, and major validation samples (84/89) are within the confidence
465 interval of 95%, indicating a high accuracy in lake mapping (Figure 9Figure 9c and d). The
466 error of 89 sample lakes is 5.48% in total area between Landsat- and Google Earth-derived
467 data, and 0.61% for Sentinel- and Google Earth-derived data. The median (±standard
468 deviation) in discrepancy of individual lake area is 7.66±4.96 % for Landsat- and Google
469 Earth-derived data, and 4.46±4.62 % for Sentinel- and Google Earth-derived data. Our glacial
470 lake dataset shows a satisfactory mapping accuracy, although Sentinel-derived lake data
471 performs more accurate than those from Landsat images. We also validated the sampling
472 Landsat-derived 89 lakes by the existing Landsat-extracted lake data produced by Wang et al.
473 (2020). A total of 83 lakes are available in Wang's data with a mean difference of 0.005 km^2

带格式的: 字体: 非加粗

带格式的: 字体: 非加粗

带格式的: 字体: 非加粗

474 in lake area (Figure A8). This also shows an improvement of our lake product in contrast to
475 the existing dataset.

476
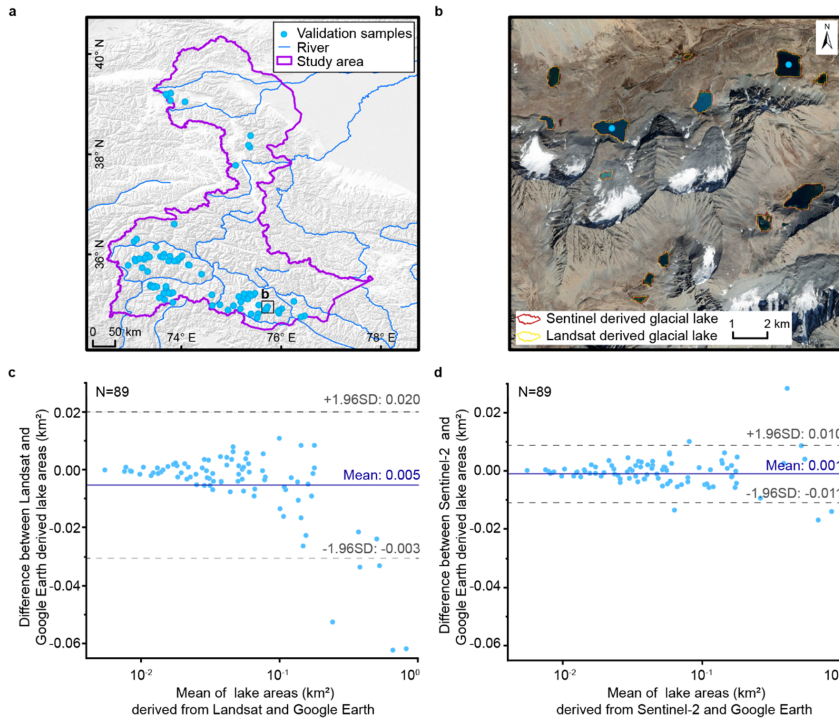
Figure 9. Distribution of the validation sample (a), visual comparison of glacial lakes derived from
Landsat and Sentinel-2 images overlaying Google Earth imagery (© Google Earth 2019) in a zoomed site
(b), and differences between our glacial lake product (mapped from Landsat and Sentinel-2 images) and
the validation reference (digitized from Google Earth images) (c and d). ~~Distribution of validation samples~~
~~(a), comparison of glacial lakes derived from Landsat and Sentinel-2 overlaying Google Earth image (©~~
~~Google Earth 2019) in a zoomed site (b), and glacial lake product validated by Google Earth derived lake~~
~~boundaries (c and d).~~

6.2 Comparison of Sentinel-2 and Landsat derived products

Glacial lakes from Landsat and Sentinel-2 images have a high consistency in number and
area with overlap rates from approximately 86% to 94% for all lakes greater than 0.0045 km^2
(Table 4~~Table 4~~), indicating a good potential for coordinated utility with Landsat archived
observation (Figure 10~~Figure 10~~). Lake extents extracted from Landsat and Sentinel images
match well for various types and sizes (Figure 10~~Figure 10~~ and Figure 11~~Figure 11~~, Table
4~~Table 4~~). The best consistency rate reaches 94% for the glacial lakes between 0.1 km^2 and
0.2 km^2. The difference in area of glacial lakes extracted from Landsat and Sentinel-2 images
generally lies within the uncertainty ranges.

带格式的: 字体: 非加粗

带格式的: 字体: 非加粗

带格式的: 字体: 非加粗

带格式的: 字体: 非加粗

带格式的: 字体: 非加粗

Landsat derived glacial lake Sentinel derived glacial lake 0 400m
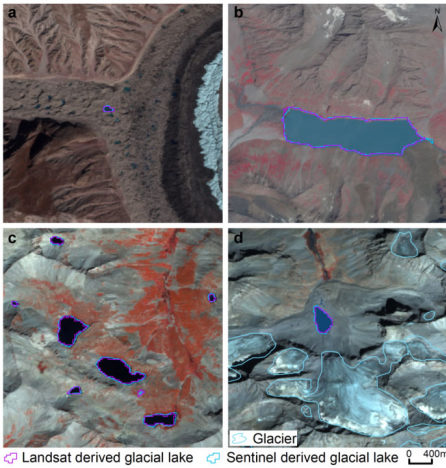
Figure 10. High consistency of lake extents extracted from Landsat and Sentinel-2 images. Lake types shown include supraglacial (a), glacier-fed moraine-dammed (b), unconnected glacial-erosion lake without glacier melt supply (c) and glacier-fed moraine-dammed lakes (d).

Spatial resolution of satellite images plays a primary role in the discrepancies in count and area of glacial lakes extracted from Landsat (30 m) and Sentinel-2 (10 m) observations. Due to a finer spatial resolution, Sentinel-2 images can extract more glacial lakes and more accurate extents than those from Landsat images. We set the same 5 pixels as the MMU for both Landsat and Sentinel-2 images, which corresponds to a minimum area of 0.0045 km^2 and 0.0005 km^2, respectively. The minimum mapping area results in generating nearly 5000 more lakes from Sentinel-2 images than from Landsat images, causing the greatest discrepancy in number (Table 4Table 4), such as Figure 11Figure 11a. Small lakes such as supraglacial lakes play an important role in analyzing glacier evolution and supraglacial drainage systems (Liu and Mayer, 2015; Miles et al., 2018), implying a potential of our dataset to be applied in studies of glacier-lake evolutions. Meanwhile, Sentinel-2 images are able to depict boundaries of glacial lake with a lower uncertainty, as for some small islands and narrow channels (Figure 11Figure 11b and c) were mapped from Sentinel-2 imagery that were unable to be detected in Landsat imagery.

In addition to the difference in image resolution, Ddifferent acquisition dates between Sentinel-2 and Landsat images can also contribute to the discrepancy of those two glacial lake datasets. Acquiring same-day images from the two sensors were not always possible due to the impacts of cloud contaminations, topographic shadows, snow cover and revisit periods (Williamson et al., 2018; Paul et al., 2020). As exemplified in Figure 11d, the mapped glacial lake areas exhibit a substantial discrepancy, which is likely a joint consequence of both sensor difference and actual glacier lake dynamics that occurred during this short period of time. Glacial lakes are changing temporally in the context of climate and glacier changes. The example is given to supraglacial lakes which showed considerable changes during a short period of time between the applied Landsat and Sentinel-2 images (Figure 11d). Despite our

522 efforts of leveraging all available high-quality images, the overlap of acquisition dates
523 between Landsat and Sentinel-2 images for the same location is relatively low (only 7 scenes
524 of Sentinel-2 images or 112 glacial lakes in 2020) in this study area, and the consequential
525 temporal gaps led to a difference in the number and area of the derived glacial lakes.
526
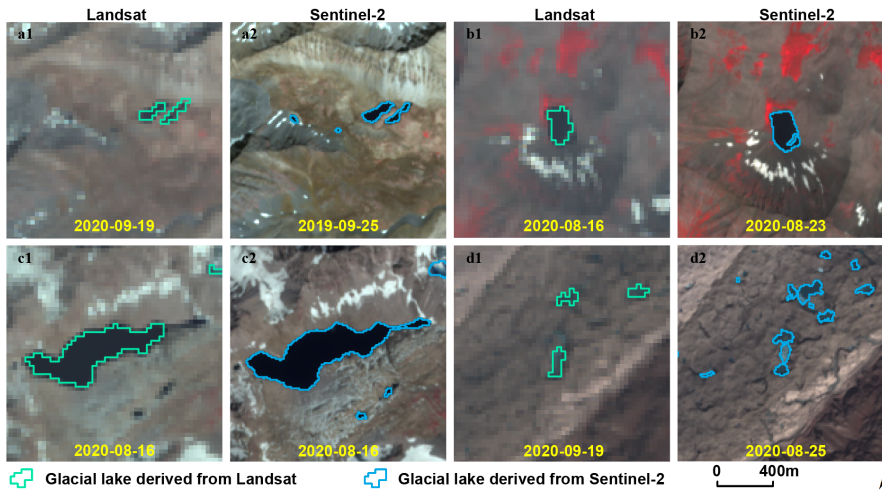
527 🏷️ Glacial lake derived from Landsat   🏷️ Glacial lake derived from Sentinel-2   0 400m   N

528 **Figure 11.** Discrepancy of lake extents extracted from Landsat and Sentinel-2 images.
529

530 6.3 Comparison with previous similar dataset

531 An increasing number of glacier lake datasets have been released over the past years, and
532 most of them were produced from long-term Landsat archives. Regional glacial lake datasets
533 using Sentinel images are scarce. Lack of Sentinel-derived glacial lake data in the study area
534 makes it impossible to compare. Here we selected four available glacial lake datasets to
535 compare with our Landsat-derived dataset.
536   We provide the latest glacial lake dataset (in 2020) and the most long-term 30-m Landsat
537 observation (1990 to 2020) for this study, with a range of critical attributes including two
538 types of classification systems. Within the same study area, our 2020 glacial lakes appear to
539 be closest to the 2018 dataset produced by Wang et al. (2020), with the highest overlap of
540 greater than 91~~85~~% in ~~area~~ count (Table 5~~Table 5~~). In Wang et al. (2020) , the minimum
541 mapping unit is 6 pixels so their dataset has a less lake quantity. However, their dataset
542 contains many large landslide-dammed lakes that are excluded in our glacial lake mapping.
543 As a result, their total glacier lake area is greater than ours. The overlapping rates between
544 Wang's glacial lakes (2020) in 1990 and ours are more than ~~76~~83% in ~~area~~count. However,
545 their results show a distinct increase of glacial lakes in number and area between 1990 and
546 2018 (Wang et al., 2020) whereas our data show a more stable change between 1990 and
547 2020. One possible reason is that manually delineating glacial lakes twice by different
548 operators during Wang's lake mapping (2020) exacerbates the errors of mapping. Another
549 reason is that their data contains landslide-dammed lakes that fluctuate greatly with time and

带格式的: 字体: 非加粗

550 expanded recently. One example is the Attabad Lake (Located at 36°18'22.33"N,
551 74°49'34.36"E).
552
553

554 **Table 5.** Comparison between our Landsat-based mapping and other third-party Landsat-based glacial lake
555 datasets in the study area.

Baseline year (period)	Method	MMU m² (pixels)	Count (km²)	Other data / our product % (%)	Reference
1990 (1988-1993)	Manual	5400 (6)	1720 (89.68±13.69)	83.13 (105.87)	Wang et al., 2020
1990 (1989-1994)	Semi-automated	5400 (6)	2069 (84.71±14.41)		This study
1990 (1990-1999)	Automated	50000 (55)	145 (20.28)	38.77 (36.98)	Shugar et al., 2020
1990 (1989-1994)	Semi-automated	50000 (55)	374 (54.84±5.49)		This study
1990 (1989-1992)	Manual	4500 (5)*	622 (51.93±10.15)	28.88 (61.02)	Zhang et al., 2015
1990 (1989-1994)	Semi-automated	4500 (5)*	2154 (85.10±14.66)		This study
2000 (1999-2001)	Manual	4500 (5)*	724 (61.41±11.91)	33.15 (71.32)	Zhang et al., 2015
2000 (1996-2004)	Semi-automated	4500 (5)*	2184 (86.10±14.83)		This study
2000 (2000-2004)	Automated	50000 (55)	155 (22.35)	42.94 (40.70)	Shugar et al., 2020
2000 (1996-2004)	Semi-automated	50000 (55)	361 (54.91±5.40)		This study
2008	Automated & Manual	8100 (9)	1067 (65.45)	59.28 (78.08)	Chen et al., 2021
2000 (1996-2004)	Semi-automated	8100 (9)	1800 (83.82±13.59)		This study
2015 (2015-2018)	Automated	50000 (55)	148 (21.45)	40.66 (39.11)	Shugar et al., 2020
2020 (2016-2020)	Semi-automated	50000 (55)	364 (54.84±5.41)		This study
2017	Automated & Manual	8100 (9)	1063 (63.23)	58.63 (75.45)	Chen et al., 2021
2020 (2016-2020)	Semi-automated	8100 (9)	1813 (83.80±13.63)		This study
2018 (2017-2018)	Manual	5400 (6)	1956 (102.46±15.48)	91.02 (119.24)	Wang et al., 2020
2020 (2016-2020)	Semi-automated	5400 (6)	2149 (85.93±14.74)		This study

556 Note: MMU represents the minimum mapping unit that is possible to enable a valid comparison between our product and each
557 of the third-party datasets. * The MMU in the dataset of Zhang et al. (2015) is 3 pixels, finer than 5 pixels in our product, so a
558 MMU threshold of 5 pixels was used for this comparison. "% (%)" represents the ratios between the third-party dataset and
559 our product in count and area, respectively.
560 Comparison of different glacial lake datasets sourced from Landsat images in the study area.

Baseline year (period)	Method	MMU m² (pixels)	Count (km²)	Other's area / ours (%)	Reference
1990 (1988-1993)	Manual	5400 (6)	1720 (89.68±13.69)	105.86	Wang et al., 2020
1990 (1990-1999)	Automated	50000 (55)	145 (20.28)	36.98	Shugar et al., 2020
1990 (1989-1992)	Manual	2700 (3)	622 (51.93±10.15)	61.02	Zhang et al., 2015
1990 (1989-1994)	Semi-automated	4500 (5)	2154 (85.10±14.66)	—	This study
2000 (1999-2001)	Manual	2700 (3)	724 (61.41±11.91)	71.32	Zhang et al., 2015
2000 (2000-2004)	Automated	50000 (55)	155 (22.35)	40.27	Shugar et al., 2020
2008	Automated & Manual	8100 (9)	1067 (65.45)	78.08	Chen et al., 2021
2000 (1996-2004)	Semi-automated	4500 (5)	2184 (86.10±14.83)	—	This study
2015 (2015-2018)	Automated	50000 (55)	148 (21.45)	38.77	Shugar et al., 2020
2017	Automated & Manual	8100 (9)	1063 (63.23)	75.47	Chen et al., 2021
2018 (2017-2018)	Manual	5400 (6)	1956 (102.46±15.48)	119.24	Wang et al., 2020

The second highest overlapping rate is approximate ~~54~~59% for 2008 and 58% for 2017 in ~~area~~ count comparing with Chen's data (Chen et al., 2021). Similarly, a minimum mapping unit of 55 pixels (50000 m^2) in Shugar et al.'s, dataset (2020) led to ~~the~~ lowes~~t~~r overlap with less than 43~~24~~% in ~~area~~count and area. The dataset from Zhang et al. (2015) shows fewer glacial lakes in 1990 and 2000 even with a smaller MMU of 3 pixels. By inspecting their dataset, we attributed this anomalous discrepancy to a range of glacial lakes that were missing due to lack of thorough cross-check quality assurance during their manual delineation. Our Landsat derived glacial lake dataset has been visually cross-checked over three time periods after the step of threshold-based semi-automated lake mapping, and also been visually validated by Sentinel-2 derived glacial lakes. Through this series of quality assurance, we aim at delivering one of the most reliable multi-decadal glacial lake products for this study area.

Other factors, such as image quality and acquisition dates, mapping methods and quality assurance workflow, might also lead to the discrepancies between the glacial lake datasets. Despite such discrepancies, an increasing number of publically-shared datasets benefit potential users to select the most suitable one for their objectives. Herein, we provide an up-to-date glacial lake dataset derived from both Landsat and Sentinel-2 observations, which further increased the availability of glacial lake dataset for water resource and GLOFs risk assessment, predicting glacier-lake evolutions (Carrivick et al., 2020) in the context of climate change.

6.4 Limitation and updating plan

We would like to acknowledge several limitations of our glacier lake dataset, largely due the availability of high quality satellite images in the study area and inadequate field survey data (Wang et al., 2020; Chen et al., 2021). First, it is unlikely to collect enough good-quality images within one calendar year for the entire study area due to high possibility of cloud or snow covers. Even though the capacity of repeat observations for Landsat-8 OLI and Sentinel-2 increased (Roy et al., 2014; Williamson et al., 2018; Wulder et al., 2019; Paul et al., 2020), the 2020 glacial lake dataset has to employ images acquired in adjacent years besides 2020. Most images used from Landsat and Sentinel-2 platforms were imaged in autumn, and some images taken between April and July and in November also were employed. Distribution and changes in glacial lakes primarily represent the characteristics between August and October. Glacial lakes evolve with time and space (Nie et al., 2017), and subtle inter- and intra-annual changes (Liu et al., 2020) for each time period were ignored. Second, field investigation data are limited due to low accessibility of high mountain environment in the study area, which restrained the accuracy in classifying the glacial lake types. Although very high-resolution Google Earth images were utilized to assist in lake type interpretation, occasional misclassification was unavoidable. We implemented two types of classification systems based on a careful utilization of glacier data, DEM, geomorphological features and expert knowledge. However, the lack of in situ survey prohibited a thorough validation of the glacial lake types. Third, the rigorous quality assurance and cross check after

603 semi-automated lake mapping assure the quality of our lake dataset but are still time and cost
604 prohibitive. State-of-the-art mapping methods, such as deep learning method (Wu et al.,
605 2020), Google Earth Engine cloud-computing (Chen et al., 2021) and synergy of SAR and
606 optical images (Wangchuk and Bolch, 2020; How et al., 2021), would be used in the future to
607 balance product accuracy and time cost.
608 The glacial lake dataset will be updated using newly collected Landsat and Sentinel
609 images at a five-year interval or modified according to user feedbacks. The updated glacial
610 lake dataset will continue to be released freely and publicly on the Mountain Science Data
611 Center sharing platform.

7 Data availability

613 Our glacial lake dataset extracted from Sentinel-2 images in 2020 and Landsat observation
614 between 1990 and 2020 are available online via the Mountain Science Data Center, the
615 Institute of Mountain Hazards and Environment, the Chinese Academy of Sciences at
616 https://doi.org/10.12380/Glaci.msdc.000001 (Lesi et al., 2022). The glacial lake dataset is
617 provided in both ESRI shapefile format (total size of 22.6 MB) and the Geopackage format
618 (version 1.2.1) with a total size of 9.2MB, which can be opened and further processed by
619 open-source geographic information system software such as QGIS.

8 Conclusions

621 Glacial lake inventories of the entire China-Pakistan Economic Corridor in 2020 were
622 provided based on Landsat and Sentinel-2 images using a threshold-based semi-automated
623 mapping method. Both Landsat and Sentinel-2 derived glacial lake dataset show similar
624 characteristics in spatial distribution and in the statistics of count and area. By contrast,
625 glacial lake dataset derived from Sentinel-2 images with a spatial resolution of 10 m has a
626 lower mapping error and more accurate lake boundary than those from 30 m spatial
627 resolution Landsat images whereas Landsat imagery is more suitable to analyze spatial-
628 temporal changes at a longer time scale due to its long-term archived observations at a
629 consistent 30 m spatial resolution starting from the late 1980s.
630 Glacial lakes in the study area remain relatively stable with a slight increase in number and
631 area between 1990 and 2020 according to Landsat observations. Our dataset reveals that 2154
632 glacial lakes in 1990 covering 85.1 ± 14.66 km^2 increased to 2234 lakes with a total area of
633 86.31 ± 14.98 km^2. The same mapping method and rigorous workflow of quality assurance
634 and quality control used in this study reduced the error in multi-temporal changes of glacial
635 lakes.
636 The Hanshaw's error estimation method for pixel-based lake mapping was improved by
637 removing repeatedly calculated edge pixels that vary with lake shape. Therefore, the newly
638 proposed method reduces the estimated value of uncertainty from satellite observations. The
639 average relative error is $\pm17.36\%$ for Landsat-derived product and $\pm8.15\%$ for product from
640 Sentinel-2.
641 Our glacial lake dataset contains a range of critical parameters that maximize their
642 potential utility for water resource and GLOFs risk evaluation, cryosphere-hydrological and
643 glacier-lake evolution projection. The dual classification systems of glacial lake types were

644 developed and are very likely to attract broader researchers and scientists to use our datasets.
645 In comparison with other existing glacial lake datasets, our products were created through a
646 thorough consideration of lake types, cross checks and rigorous quality assurance, and will be
647 updated and released continuously in the Mountain Science Data Center. As such, we expect
648 that our glacial lake dataset will have significant value to cryospheric-hydrology research, the
649 assessment of water resource and glacier-related hazards in the CPEC.
650
651 **Appendix.** The appendix related to this article is available online.
652
653 **Author contributions.** ML and YN conceived the study, ML, YN and XD performed data
654 processing and analysis of the glacial lake inventory data, JW contributed to tool
655 development and mapping methods, ML and YN wrote the manuscript. All authors reviewed
656 and edited the manuscript before submission.
657
658 **Competing interests.** The authors declare no conflict of interest.
659

660 **Acknowledgements.**
661 We are grateful for the editor Kenneth Mankoff and three anonymous referees for their
662 constructive comments that greatly help us to improve this manuscript. This study was
663 supported by the second Tibetan Plateau Scientific Expedition and Research Program (grant
664 2019QZKK0603), the National Natural Science Foundation of China (Grant Nos. 42171086,
665 41971153), the International Science & Technology Cooperation Program of China (No.
666 2018YFE0100100), the Chinese Academy of Sciences "Light of West China" and Natural
667 Sciences and Engineering Research Council of Canada (Grant No. DG-2020-04207).

668
669

670 **Appendix**

671 **Tutorial for Improved Uncertainty Estimating Method**

672

673 The Hanshaw's equation was originally proposed for pixelated polygons (such as a polygon
674 directly extracted from a remote sensing image), and performed more robustly than manually
675 digitized polygons (where vertices do not necessarily follow the pixel edges). Our improved
676 method also performs better for pixelated polygons. This tutorial is dedicated to helping
677 implement our improved uncertainty estimation method.

678

679 **Procedure of uncertainty estimating method (using ArcGIS (© ESRI) for example)**
680 1. Removing redundant nodes (optional)
681 We found that a small proportion (~1%) of the pixelated lake polygons (directly extracted
682 from satellite images) have redundant nodes, which affects the value of inner nodes. If no
683 redundant nodes exist, this step can be skipped. Or, we recommend using the "Simplify
684 Polygon" tool in ArcGIS to remove those nodes (Figure A1~~Figure A1~~).
685   In the Simplify Polygon panel
686 ●   Input your dataset.
687 ●   Set the output path and output file name.
688 ●   Choose the simplification algorithm. We recommended "POINT_REMOVE".
689 ●   Set the tolerance of simplification algorithm. In this step, we need to ensure that the
690   polygon boundaries remain unchanged after deleting redundant nodes. Generally, a
691   tolerance of 1 meter will suffice, or you can adjust the threshold until your satisfaction.
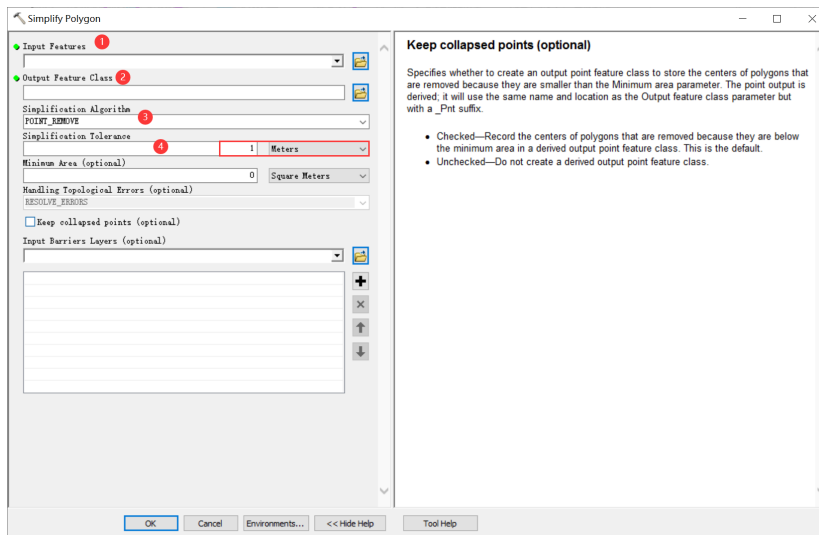
692

693 **Figure A1.** Input and option for Simplify Polygon in ArcGIS.

694

695 2. Calculating the total number of nodes using ArcGIS (Figure A2~~Figure A2~~):

696 ● Add a new field in the attribute table of dataset.
697 ● Open Field Calculator.
698 ● Switch the parser to python mode, and enter the following code "!shape.pointcount!" in
699   the blue box to calculate the total number of nodes for each glacial lake boundary.
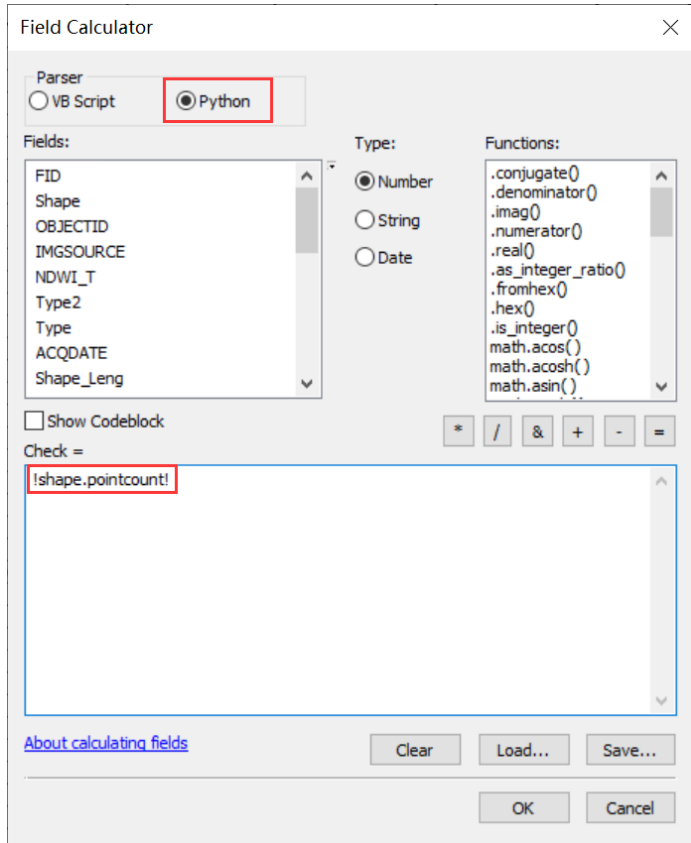
700
701 **Figure A2.** Total node calculation in ArcGIS.
702
703 3. Calculating the number of inner nodes:
704
705 For polygons without islands (Figure A3~~Figure A3~~), use the equation 5. An inner node is a

706 polygon vertex where the interior angle surrounding it is greater than 180 degrees. An outer
707 node is the opposite of the inner node, where the interior angle is less than 180 degrees. We
708 found that the outer nodes are usually four more than the inner nodes in our glacial lake
709 dataset. The total nodes in ArcGIS contain one overlapping node to close the polygon,
710 meaning the endpoint is also the startpoint. This extra count was deleted in the calculation
711 (equation 5).

712
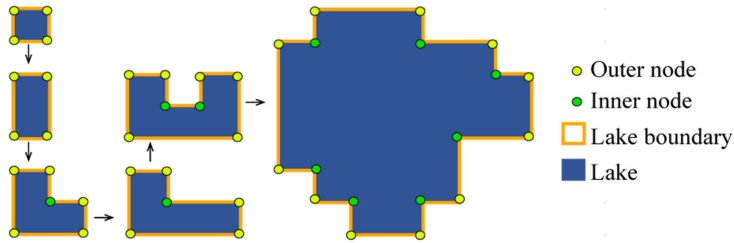
713
714
Figure A3. Sketch of outer and inner nodes of various glacial lakes without island.

715

716 For polygons with island (Figure A4Figure A4) use the equation 6.

717
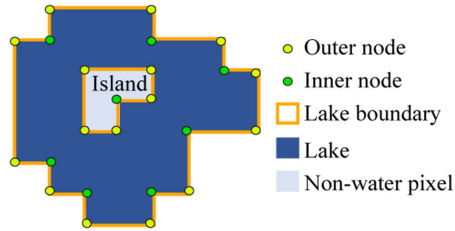
718
719
Figure A4. Sketch of outer and inner nodes for glacial lake with island.

720

721 We further specify the steps below to help implement equation 6.

722

723 Sept 1: detect the number of islands within each polygon.

724 ● Convert the initial lake polygon to polyline using the "Feature To Line" tool (Figure
725 A5Figure A5).

726
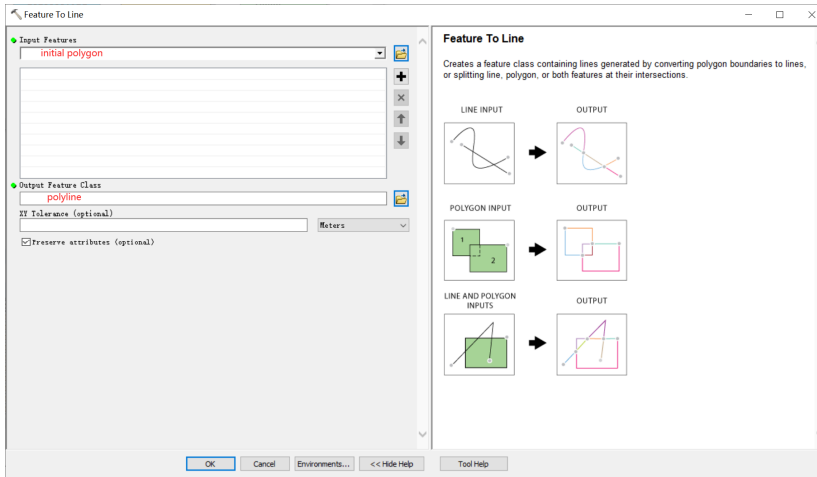
Figure A5. Feature To Line tool in ArcGIS

728

729 ● Convert the polyline to generate a new polygon (Figure A6~~Figure A6~~).

730
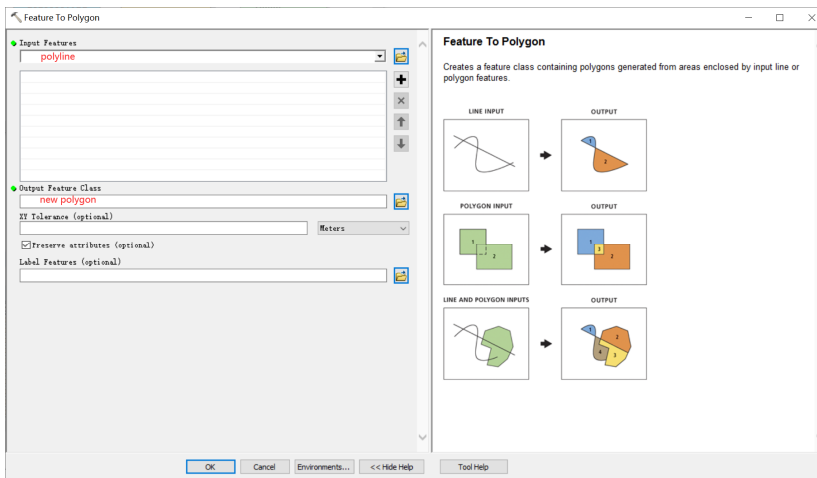
Figure A6. Feature To Polygon tool in ArcGIS

732

733 ● Erase the new polygon by the initial polygon, which outputs the islands. Then we can
734 count how many islands there are in each lake (Figure A7~~Figure A7~~).
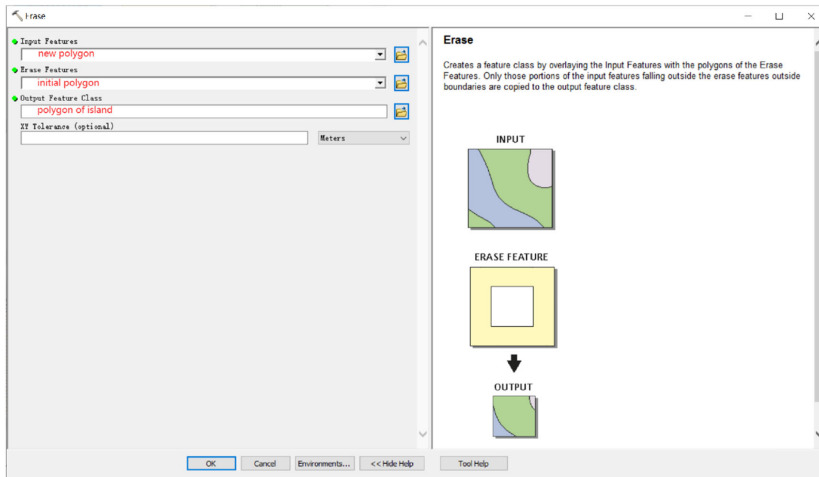
735
736 **Figure A7.** Erase tool in ArcGIS.
737
738 Step 2: calculate the number of inner nodes for each polygon with island using equation 6.
739
740 4. Calculating the uncertainty of lake mapping using equation 4.
741
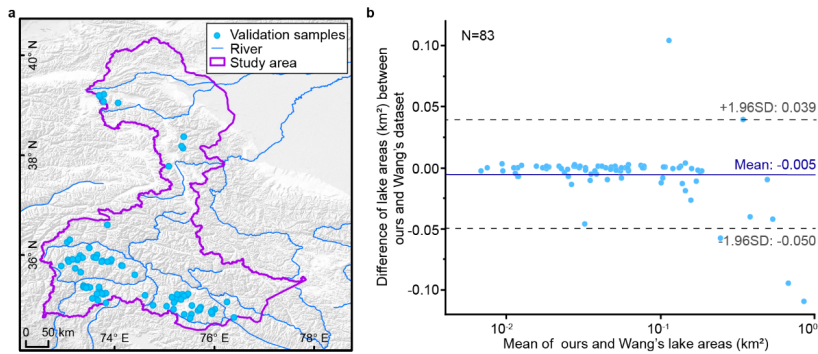
742
743 **Figure A8.** Distribution of validation samples (a) and comparison of glacial lakes (b) derived from our
744 Landsat product in 2020 and Wang's lake data in 2018.
745

746 **References**

747 Ashraf, A., Naz, R., Iqbal, M.B.: Altitudinal dynamics of glacial lakes under changing climate in the Hindu

748 Kush, Karakoram, and Himalaya ranges. Geomorphology, 283: 72-79,

749 https://doi.org/10.1016/j.geomorph.2017.01.033, 2017.

750 Azam, M.F., Kargel, J.S., Shea, J.M., Nepal, S., Haritashya, U.K., Srivastava, S., Maussion, F., Qazi, N.,

751 Chevallier, P., Dimri, A.P., Kulkarni, A.V., Cogley, J.G., Bahuguna, I.: Glaciohydrology of the Himalaya-

752 Karakoram. Science, 373: eabf3668, https://doi.org/10.1126/science.abf3668, 2021.

753 Battamo, A.Y., Varis, O., Sun, P., Yang, Y., Oba, B.T., Zhao, L.: Mapping socio-ecological resilience along the

754 seven economic corridors of the Belt and Road Initiative. J. Clean. Prod., 309: 127341,

755 https://doi.org/10.1016/j.jclepro.2021.127341, 2021.

756 Bhambri, R., Hewitt, K., Kawishwar, P., Kumar, A., Verma, A., Snehmani, Tiwari, S., Misra, A.: Ice-dams,

757 outburst floods, and movement heterogeneity of glaciers, Karakoram. Global Planet. Change, 180: 100-116,

758 https://doi.org/10.1016/j.gloplacha.2019.05.004, 2019.

759 Bhattacharya, A., Bolch, T., Mukherjee, K., King, O., Menounos, B., Kapitsa, V., Neckel, N., Yang, W., Yao,

760 T.: High Mountain Asian glacier response to climate revealed by multi-temporal satellite observations since the

761 1960s. Nat. Commun., 12: 4133, https://doi.org/10.1038/s41467-021-24180-y, 2021.

762 Bolch, T., Pieczonka, T., Mukherjee, K., Shea, J.: Brief communication: Glaciers in the Hunza catchment

763 (Karakoram) have been nearly in balance since the 1970s. The Cryosphere, 11: 531-539,

764 https://doi.org/10.5194/tc-11-531-2017, 2017.

765 Brun, F., Berthier, E., Wagnon, P., Kääb, A., Treichler, D.: A spatially resolved estimate of High Mountain Asia

766 glacier mass balances from 2000 to 2016. Nat. Geosci., 10: 668-673, https://doi.org/10.1038/ngeo2999, 2017.

767 Brun, F., Wagnon, P., Berthier, E., Jomelli, V., Maharjan, S.B., Shrestha, F., Kraaijenbrink, P.D.A.:

768 Heterogeneous Influence of Glacier Morphology on the Mass Balance Variability in High Mountain Asia.

769 Journal of Geophysical Research: Earth Surface, 124: 1331-1345, https://doi.org/10.1029/2018JF004838, 2019.

770 Carrivick, J.L., Tweed, F.S.: Proglacial lakes: character, behaviour and geological importance. Quaternary Sci.

771 Rev., 78: 34-52, https://doi.org/10.1016/j.quascirev.2013.07.028, 2013.

772 Carrivick, J.L., Quincey, D.J.: Progressive increase in number and volume of ice-marginal lakes on the western

773 margin of the Greenland Ice Sheet. Global Planet. Change, 116: 156-163,

774 https://doi.org/10.1016/j.gloplacha.2014.02.009, 2014.

775 Carrivick, J.L., Tweed, F.S.: A global assessment of the societal impacts of glacier outburst floods. Global

776 Planet. Change, 144: 1-16, https://doi.org/10.1016/j.gloplacha.2016.07.001, 2016.

777 Carrivick, J.L., Tweed, F.S., Sutherland, J.L., Mallalieu, J.: Toward Numerical Modeling of Interactions

778 Between Ice-Marginal Proglacial Lakes and Glaciers. Frontiers in Earth Science, 8,

779 https://doi.org/10.3389/feart.2020.577068, 2020.

780 Carrivick, J.L., How, P., Lea, J.M., Sutherland, J.L., Grimes, M., Tweed, F.S., Cornford, S., Quincey, D.J.,

781 Mallalieu, J.: Ice-Marginal Proglacial Lakes Across Greenland: Present Status and a Possible Future. Geophys.

782 Res. Lett., 49: e2022GL099276, https://doi.org/https://doi.org/10.1029/2022GL099276, 2022.

783 Chen, F., Zhang, M., Guo, H., Allen, S., Kargel, J.S., Haritashya, U.K., Watson, C.S.: Annual 30 m dataset for

784 glacial lakes in High Mountain Asia from 2008 to 2017. Earth System Science Data, 13: 741-766,

785 https://doi.org/10.5194/essd-13-741-2021, 2021.

786 Chen, X., Cui, P., You, Y., Cheng, Z., Khan, A., Ye, C., Zhang, S.: Dam-break risk analysis of the Attabad

787 landslide dam in Pakistan and emergency countermeasures. Landslides, 14: 675-683,

788 https://doi.org/10.1007/s10346-016-0721-7, 2017.

789 Cook, S.J., Quincey, D.J.: Estimating the volume of Alpine glacial lakes. Earth Surf. Dynam., 3: 559-575,

790 https://doi.org/10.5194/esurf-3-559-2015, 2015.

791 Emmer, A., Cuřín, V.: Can a dam type of an alpine lake be derived from lake geometry? A negative result. J.

792 Mt. Sci.-Engl., 18: 614-621, https://doi.org/10.1007/s11629-020-6003-9, 2021.

793   Farr, T.G., Rosen, P.A., Caro, E., Crippen, R., Duren, R., Hensley, S., Kobrick, M., Paller, M., Rodriguez, E.,

794   Roth, L., Seal, D., Shaffer, S., Shimada, J., Umland, J., Werner, M., Oskin, M., Burbank, D., Alsdorf, D.: The

795   Shuttle Radar Topography Mission. Rev. Geophys., 45: RG2004, https://doi.org/10.1029/2005RG000183, 2007.

796   Gardelle, J., Arnaud, Y., Berthier, E.: Contrasted evolution of glacial lakes along the Hindu Kush Himalaya

797   mountain range between 1990 and 2009. Global Planet. Change, 75: 47-55,

798   https://doi.org/10.1016/j.gloplacha.2010.10.003, 2011.

799   Hanshaw, M.N., Bookhagen, B.: Glacial areas, lake areas, and snow lines from 1975 to 2012: status of the

800   Cordillera Vilcanota, including the Quelccaya Ice Cap, northern central Andes, Peru. The Cryosphere, 8: 359-

801   376, https://doi.org/10.5194/tc-8-359-2014, 2014.

802   Hewitt, K.: The Karakoram Anomaly? Glacier Expansion and the 'Elevation Effect,' Karakoram Himalaya. Mt.

803   Res. Dev., 25: 332-340, https://doi.org/10.1659/0276-4741(2005)025[0332:TKAGEA]2.0.CO;2, 2005.

804   Hewitt, K., 2014. Glaciers of the Karakoram Himalaya:Glacial Environments, Processes, Hazards and

805   Resources. Springer, Dordrecht.

806   How, P., Messerli, A., Mätzler, E., Santoro, M., Wiesmann, A., Caduff, R., Langley, K., Bojesen, M.H., Paul,

807   F., Kääb, A., Carrivick, J.L.: Greenland-wide inventory of ice marginal lakes using a multi-method approach.

808   Sci. Rep.-UK, 11: 4481, https://doi.org/10.1038/s41598-021-83509-1, 2021.

809   Huggel, C., Kääb, A., Haeberli, W., Teysseire, P., Paul, F.: Remote sensing based assessment of hazards from

810   glacier lake outbursts: a case study in the Swiss Alps. Can. Geotech. J., 39: 316-330,

811   https://doi.org/10.1139/t01-099, 2002.

812   Hugonnet, R., Mcnabb, R., Berthier, E., Menounos, B., Nuth, C., Girod, L., Farinotti, D., Huss, M., Dussaillant,

813   I., Brun, F., Kääb, A.: Accelerated global glacier mass loss in the early twenty-first century. Nature, 592: 726-

814   731, https://doi.org/10.1038/s41586-021-03436-z, 2021.

815   Huss, M., Hock, R.: Global-scale hydrological response to future glacier mass loss. Nat. Clim. Change, 8: 135-

816   140, https://doi.org/10.1038/s41558-017-0049-x, 2018.

817   Immerzeel, W.W., Lutz, A.F., Andrade, M., Bahl, A., Biemans, H., Bolch, T., Hyde, S., Brumby, S., Davies,

818   B.J., Elmore, A.C., Emmer, A., Feng, M., Fernández, A., Haritashya, U., Kargel, J.S., Koppes, M.,

819   Kraaijenbrink, P.D.A., Kulkarni, A.V., Mayewski, P.A., Nepal, S., Pacheco, P., Painter, T.H., Pellicciotti, F.,

820   Rajaram, H., Rupper, S., Sinisalo, A., Shrestha, A.B., Viviroli, D., Wada, Y., Xiao, C., Yao, T., Baillie, J.E.M.:

821   Importance and vulnerability of the world's water towers. Nature, 577: 364-369, https://doi.org/10.1038/s41586-

822   019-1822-y, 2020.

823   Jarvis, A., Reuter, H.I., Nelson, A., Guevara, E., 2008. Hole-filled seamless SRTM data V4. 2008, International

824   Centre for Tropical Agriculture (CIAT), available from http://srtm.csi.cgiar.org.

825   Jiang, S., Nie, Y., Liu, Q., Wang, J., Liu, L., Hassan, J., Liu, X., Xu, X.: Glacier Change, Supraglacial Debris

826   Expansion and Glacial Lake Evolution in the Gyirong River Basin, Central Himalayas, between 1988 and 2015.

827   Remote Sens.-Basel, 10: 986, https://doi.org/10.3390/rs10070986, 2018.

828   Kääb, A., Berthier, E., Nuth, C., Gardelle, J., Arnaud, Y.: Contrasting patterns of early twenty-first-century

829   glacier mass change in the Himalayas. Nature, 488: 495-498, https://doi.org/10.1038/nature11324, 2012.

830   Lesi, M., Nie, Y., Shugar, D.H., Wang, J., Deng, Q., Chen, H.: Landsat and Sentinel-derived glacial lake dataset

831   in the China-Pakistan Economic Corridor from 1990 to 2020. Mountain Science Data Center,

832   https://doi.org/10.12380/Glaci.msdc.000001   CSTR:1a006.11.Glaci.msdc.000001, 2022.

833   Li, D., Shangguan, D., Anjum, M.N.: Glacial Lake Inventory Derived from Landsat 8 OLI in 2016–2018 in

834   China–Pakistan Economic Corridor. ISPRS international journal of geo-information, 9: 294,

835   https://doi.org/10.3390/ijgi9050294, 2020.

836   Li, Z., Deng, X., Zhang, Y.: Evaluation and convergence analysis of socio-economic vulnerability to natural

837   hazards of Belt and Road Initiative countries. J. Clean. Prod., 282: 125406,

838   https://doi.org/10.1016/j.jclepro.2020.125406, 2021.

839   Liu, Q., Mayer, C.: Distribution and interannual variability of supraglacial lakes on debris-covered glaciers in

840   the Khan Tengri-Tumor Mountains, Central Asia. Environ. Res. Lett., 10: 014014 2015.

841   Liu, Q., Mayer, C., Wang, X., Nie, Y., Wu, K., Wei, J., Liu, S.: Interannual flow dynamics driven by frontal

842   retreat of a lake-terminating glacier in the Chinese Central Himalaya. Earth Planet. Sc. Lett., 546: 116450,

843   https://doi.org/10.1016/j.epsl.2020.116450, 2020.

844   Lyons, E.A., Sheng, Y., Smith, L.C., Li, J., Hinkel, K.M., Lenters, J.D., Wang, J.: Quantifying sources of error

845   in multitemporal multisensor lake mapping. Int. J. Remote Sens., 34: 7887-7905,

846   https://doi.org/10.1080/01431161.2013.827343, 2013.

847   Martín, C.N.S., Ponce, J.F., Montes, A., Balocchi, L.D., Gorza, C., Andrea, C.: Proglacial landform assemblage

848   in a rapidly retreating cirque glacier due to temperature increase since 1970, Fuegian Andes, Argentina.

849   Geomorphology, 390: 107861, https://doi.org/10.1016/j.geomorph.2021.107861, 2021.

850   Maurer, J.M., Schaefer, J.M., Rupper, S., Corley, A.: Acceleration of ice loss across the Himalayas over the past

851   40 years. Science Advances, 5: eaav7266, https://doi.org/10.1126/sciadv.aav7266, 2019.

852   Mcfeeters, S.K.: The use of the Normalized Difference Water Index (NDWI) in the delineation of open water

853   features. Int. J. Remote Sens., 17: 1425 - 1432 1996.

854   Miles, E.S., Watson, C.S., Brun, F., Berthier, E., Esteves, M., Quincey, D.J., Miles, K.E., Hubbard, B., Wagnon,

855   P.: Glacial and geomorphic effects of a supraglacial lake drainage and outburst event, Everest region, Nepal

856   Himalaya. The Cryosphere, 12: 3891-3905, https://doi.org/10.5194/tc-12-3891-2018, 2018.

857   Nie, Y., Zhang, Y., Liu, L., Zhang, J.: Glacial change in the vicinity of Mt. Qomolangma (Everest), central high

858   Himalayas since 1976. J. Geogr. Sci., 20: 667-686, https://doi.org/10.1007/s11442-010-0803-8, 2010.

859   Nie, Y., Sheng, Y., Liu, Q., Liu, L., Liu, S., Zhang, Y., Song, C.: A regional-scale assessment of Himalayan

860   glacial lake changes using satellite observations from 1990 to 2015. Remote Sens. Environ., 189: 1-13,

861   https://doi.org/10.1016/j.rse.2016.11.008, 2017.

862   Nie, Y., Liu, Q., Wang, J., Zhang, Y., Sheng, Y., Liu, S.: An inventory of historical glacial lake outburst floods

863   in the Himalayas based on remote sensing observations and geomorphological analysis. Geomorphology, 308:

864   91-106, https://doi.org/10.1016/j.geomorph.2018.02.002, 2018.

865   Nie, Y., Liu, W., Liu, Q., Hu, X., Westoby, M.J.: Reconstructing the Chongbaxia Tsho glacial lake outburst

866   flood in the Eastern Himalaya: Evolution, process and impacts. Geomorphology, 370: 107393,

867   https://doi.org/10.1016/j.geomorph.2020.107393, 2020.

868   Nie, Y., Pritchard, H.D., Liu, Q., Hennig, T., Wang, W., Wang, X., Liu, S., Nepal, S., Samyn, D., Hewitt, K.,

869   Chen, X.: Glacial change and hydrological implications in the Himalaya and Karakoram. Nature Reviews Earth

870   & Environment, 2: 91-106, https://doi.org/10.1038/s43017-020-00124-w, 2021.

871   Paul, F., Rastner, P., Azzoni, R.S., Diolaiuti, G., Fugazza, D., Le Bris, R., Nemec, J., Rabatel, A., Ramusovic,

872   M., Schwaizer, G., Smiraglia, C.: Glacier shrinkage in the Alps continues unabated as revealed by a new glacier

873   inventory from Sentinel-2. Earth System Science Data, 12: 1805-1821, https://doi.org/10.5194/essd-12-1805-

874   2020, 2020.

875   Pfeffer, W.T., Arendt, A.A., Bliss, A., Bolch, T., Cogley, J.G., Gardner, A.S., Hagen, J., Hock, R., Kaser, G.,

876   Kienholz, C., Miles, E.S., Moholdt, G., Mölg, N., Paul, F., Radić, V., Rastner, P., Raup, B.H., Rich, J., Sharp,

877   M.J.: The Randolph Glacier Inventory: a globally complete inventory of glaciers. J. Glaciol., 60: 537-552,

878   https://doi.org/10.3189/2014JoG13J176, 2014.

879   Post, A., Mayo, L.R., 1971. Glacier dammed lakes and outburst floods in Alaska: U.S. Geological Survey

880   Hydrologic Investigations Atlas 455, U.S. Geological Survey.

881   Pritchard, H.D.: Asia's shrinking glaciers protect large populations from drought stress. Nature, 569: 649-654,

882   https://doi.org/10.1038/s41586-019-1240-1, 2019.

883   Quincey, D.J., Richardson, S.D., Luckman, A., Lucas, R.M., Reynolds, J.M., Hambrey, M.J., Glasser, N.F.:

884   Early recognition of glacial lake hazards in the Himalaya using remote sensing datasets. Global Planet. Change,

885   56: 137-152, https://doi.org/10.1016/j.gloplacha.2006.07.013, 2007.

886   Rabus, B., Eineder, M., Roth, A., Bamler, R.: The shuttle radar topography mission—a new class of digital

887   elevation models acquired by spaceborne radar. ISPRS J. Photogramm., 57: 241-262,

888   https://doi.org/10.1016/S0924-2716(02)00124-7, 2003.

889   RGI Consortium: Randolph Glacier Inventory – A Dataset of Global Glacier Outlines: Version 6.0: Technical

890   Report, https://doi.org/10.7265/N5-RGI-60, 2017.

891   Rick, B., Mcgrath, D., Armstrong, W., Mccoy, S.W.: Dam type and lake location characterize ice-marginal lake

892   area change in Alaska and NW Canada between 1984 and 2019. The Cryosphere, 16: 297-314,

893   https://doi.org/10.5194/tc-16-297-2022, 2022.

894   Rose, A., Mckee, J., Sims, K., Bright, E., Reith, A., Urban, M.: LandScan Global 2020,

895   https://doi.org/https://doi.org/10.48690/1523378, 2021.

896   Rounce, D.R., Hock, R., Shean, D.E.: Glacier Mass Change in High Mountain Asia Through 2100 Using the

897   Open-Source Python Glacier Evolution Model (PyGEM). Frontiers in Earth Science, 7: 331,

898   https://doi.org/10.3389/feart.2019.00331, 2020.

899   Roy, D.P., Wulder, M.A., Loveland, T.R., C. E., W., Allen, R.G., Anderson, M.C., Helder, D., Irons, J.R.,

900   Johnson, D.M., Kennedy, R., Scambos, T.A., Schaaf, C.B., Schott, J.R., Sheng, Y., Vermote, E.F., Belward,

901 A.S., Bindschadler, R., Cohen, W.B., Gao, F., Hipple, J.D., Hostert, P., Huntington, J., Justice, C.O., Kilic, A.,

902 Kovalskyy, V., Lee, Z.P., Lymburner, L., Masek, J.G., Mccorkel, J., Shuai, Y., Trezza, R., Vogelmann, J.,

903 Wynne, R.H., Zhu, Z.: Landsat-8: Science and product vision for terrestrial global change research. Remote

904 Sens. Environ., 145: 154-172, https://doi.org/10.1016/j.rse.2014.02.001, 2014.

905 Sakai, A.: Brief communication: Updated GAMDAM glacier inventory over high-mountain Asia. The

906 Cryosphere, 13: 2043-2049, https://doi.org/10.5194/tc-13-2043-2019, 2019.

907 Salerno, F., Thakuri, S., D'Agata, C., Smiraglia, C., Manfredi, E.C., Viviano, G., Tartari, G.: Glacial lake

908 distribution in the Mount Everest region: Uncertainty of measurement and conditions of formation. Global

909 Planet. Change, 92-93: 30-39 2012.

910 Shean, D.E., Bhushan, S., Montesano, P., Rounce, D.R., Arendt, A., Osmanoglu, B.: A Systematic, Regional

911 Assessment of High Mountain Asia Glacier Mass Balance. Frontiers in Earth Science, 7: 363,

912 https://doi.org/10.3389/feart.2019.00363, 2020.

913 Sheng, Y., Song, C., Wang, J., Lyons, E.A., Knox, B.R., Cox, J.S., Gao, F.: Representative lake water extent

914 mapping at continental scales using multi-temporal Landsat-8 imagery. Remote Sens. Environ., 185: 129-141,

915 https://doi.org/10.1016/j.rse.2015.12.041, 2016.

916 Shugar, D.H., Burr, A., Haritashya, U.K., Kargel, J.S., Watson, C.S., Kennedy, M.C., Bevington, A.R., Betts,

917 R.A., Harrison, S., Strattman, K.: Rapid worldwide growth of glacial lakes since 1990. Nat. Clim. Change, 10:

918 939-945, https://doi.org/10.1038/s41558-020-0855-4, 2020.

919 Shugar, D.H., Jacquemart, M., Shean, D., Bhushan, S., Upadhyay, K., Sattar, A., Schwanghart, W., Mcbride, S.,

920 de Vries, M., Mergili, M., Emmer, A., Deschamps-Berger, C., Mcdonnell, M., Bhambri, R., Allen, S., Berthier,

921 E., Carrivick, J.L., Clague, J.J., Dokukin, M., Dunning, S.A., Frey, H., Gascoin, S., Haritashya, U.K., Huggel,

922 C., Kaab, A., Kargel, J.S., Kavanaugh, J.L., Lacroix, P., Petley, D., Rupper, S., Azam, M.F., Cook, S.J., Dimri,

923   A.P., Eriksson, M., Farinotti, D., Fiddes, J., Gnyawali, K.R., Harrison, S., Jha, M., Koppes, M., Kumar, A.,

924   Leinss, S., Majeed, U., Mal, S., Muhuri, A., Noetzli, J., Paul, F., Rashid, I., Sain, K., Steiner, J., Ugalde, F.,

925   Watson, C.S., Westoby, M.J.: A massive rock and ice avalanche caused the 2021 disaster at Chamoli, Indian

926   Himalaya. Science, 373: 300-306, https://doi.org/10.1126/science.abh4455, 2021.

927   Ullah, S., You, Q., Ali, A., Ullah, W., Jan, M.A., Zhang, Y., Xie, W., Xie, X.: Observed changes in maximum

928   and minimum temperatures over China- Pakistan economic corridor during 1980–2016. Atmos. Res., 216: 37-

929   51, https://doi.org/10.1016/j.atmosres.2018.09.020, 2019.

930   Viviroli, D., Kummu, M., Meybeck, M., Kallio, M., Wada, Y.: Increasing dependence of lowland populations

931   on mountain water resources. Nature Sustainability, 3: 917-928, https://doi.org/10.1038/s41893-020-0559-9,

932   2020.

933   Wang, J., Sheng, Y., Tong, T.S.D.: Monitoring decadal lake dynamics across the Yangtze Basin downstream of

934   Three Gorges Dam. Remote Sens. Environ., 152: 251-269, https://doi.org/10.1016/j.rse.2014.06.004, 2014.

935   Wang, J., Sheng, Y., Wada, Y.: Little impact of the Three Gorges Dam on recent decadal lake decline across

936   China's Yangtze Plain. Water Resour. Res., 53: 3854-3877, https://doi.org/10.1002/2016WR019817, 2017.

937   Wang, J., Song, C., Reager, J.T., Yao, F., Famiglietti, J.S., Sheng, Y., Macdonald, G.M., Brun, F., Schmied,

938   H.M., Marston, R.A., Wada, Y.: Recent global decline in endorheic basin water storages. Nat. Geosci., 11: 926-

939   932, https://doi.org/10.1038/s41561-018-0265-7, 2018.

940   Wang, X., Ding, Y., Liu, S., Jiang, L., Wu, K., Jiang, Z., Guo, W.: Changes of glacial lakes and implications in

941   Tian Shan, Central Asia, based on remote sensing data from 1990 to 2010. Environ. Res. Lett., 8: 44052,

942   https://doi.org/10.1088/1748-9326/8/4/044052, 2013.

943   Wang, X., Liu, S., Zhang, J.: A new look at roles of the cryosphere in sustainable development. Advances in

944   Climate Change Research, 10: 124-131, https://doi.org/10.1016/j.accre.2019.06.005, 2019.

945 Wang, X., Guo, X., Yang, C., Liu, Q., Wei, J., Zhang, Y., Liu, S., Zhang, Y., Jiang, Z., Tang, Z.: Glacial lake

946 inventory of high-mountain Asia in 1990 and 2018 derived from Landsat images. Earth System Science Data,

947 12: 2169-2182, https://doi.org/10.5194/essd-12-2169-2020, 2020.

948 Wangchuk, S., Bolch, T.: Mapping of glacial lakes using Sentinel-1 and Sentinel-2 data and a random forest

949 classifier: Strengths and challenges. Science of Remote Sensing, 2: 100008,

950 https://doi.org/https://doi.org/10.1016/j.srs.2020.100008, 2020.

951 Westoby, M.J., Glasser, N.F., Brasington, J., Hambrey, M.J., Quincey, D.J., Reynolds, J.M.: Modelling outburst

952 floods from moraine-dammed glacial lakes. Earth-Sci. Rev., 134: 137-159,

953 https://doi.org/10.1016/j.earscirev.2014.03.009, 2014.

954 Williamson, A.G., Banwell, A.F., Willis, I.C., Arnold, N.S.: Dual-satellite (Sentinel-2 and Landsat 8) remote

955 sensing of supraglacial lakes in Greenland. The Cryosphere, 12: 3045-3065, https://doi.org/10.5194/tc-12-3045-

956 2018, 2018.

957 Wu, R., Liu, G., Zhang, R., Wang, X., Li, Y., Zhang, B., Cai, J., Xiang, W.: A Deep Learning Method for

958 Mapping Glacial Lakes from the Combined Use of Synthetic-Aperture Radar and Optical Satellite Images.

959 Remote Sens.-Basel, 12: 4020

960   2020.

961 Wulder, M.A., Loveland, T.R., Roy, D.P., Crawford, C.J., Masek, J.G., Woodcock, C.E., Allen, R.G.,

962 Anderson, M.C., Belward, A.S., Cohen, W.B., Dwyer, J., Erb, A., Gao, F., Griffiths, P., Helder, D., Hermosilla,

963 T., Hipple, J.D., Hostert, P., Hughes, M.J., Huntington, J., Johnson, D.M., Kennedy, R., Kilic, A., Li, Z.,

964 Lymburner, L., Mccorkel, J., Pahlevan, N., Scambos, T.A., Schaaf, C., Schott, J.R., Sheng, Y., Storey, J.,

965 Vermote, E., Vogelmann, J., White, J.C., Wynne, R.H., Zhu, Z.: Current status of Landsat program, science, and

966 applications. Remote Sens. Environ., 225: 127-147, https://doi.org/https://doi.org/10.1016/j.rse.2019.02.015,

967 2019.

968 Yao, C., Wang, X., Zhao, X., Wei, J., Zhang, Y.: Temporal and Spatial Changes of Glacial Lakes in the China-

969 Pakistan Economic Corridor from 1990 to 2018. Journal of Glaciology and Geocryology, 42: 33-42,

970 https://doi.org/https://doi.org/10.7522/j.issn.1000-0240.2020.0009, 2020.

971 Yao, T., Thompson, L., Yang, W., Yu, W.S., Gao, Y., Guo, X.J., Yang, X.X., Duan, K.Q., Zhao, H.B., Xu,

972 B.Q., Pu, J.C., Lu, A.X., Xiang, Y., Kattel, D.B., Joswiak, D.: Different glacier status with atmospheric

973 circulations in Tibetan Plateau and surroundings. Nat. Clim. Change, 2: 663-667,

974 https://doi.org/10.1038/NCLIMATE1580, 2012.

975 Yao, X., Liu, S., Han, L., Sun, M., Zhao, L.: Definition and classification system of glacial lake for inventory

976 and hazards study. J. Geogr. Sci., 28: 193-205, https://doi.org/10.1007/s11442-018-1467-z, 2018.

977 Zhang, G., Yao, T., Xie, H., Wang, W., Yang, W.: An inventory of glacial lakes in the Third Pole region and

978 their changes in response to global warming. Global Planet. Change, 131: 148-157,

979 https://doi.org/10.1016/j.gloplacha.2015.05.013, 2015.

980 Zhang, M., Chen, F., Tian, B.: An automated method for glacial lake mapping in High Mountain Asia using

981 Landsat 8 imagery. J. Mt. Sci.-Engl., 15: 13-24, https://doi.org/10.1007/s11629-017-4518-5, 2018.

982 Zhao, W., Xiong, D., Wen, F., Wang, X.: Lake area monitoring based on land surface temperature in the Tibetan

983 Plateau from 2000 to 2018. Environ. Res. Lett., 15, https://doi.org/10.1088/1748-9326/ab9b41, 2020.

984 Zheng, G., Allen, S.K., Bao, A., Ballesteros-Cánovas, J.A., Huss, M., Zhang, G., Li, J., Yuan, Y., Jiang, L., Yu,

985 T., Chen, W., Stoffel, M.: Increasing risk of glacial lake outburst floods from future Third Pole deglaciation.

986 Nat. Clim. Change, 11: 411-417, https://doi.org/10.1038/s41558-021-01028-3, 2021.

987